Advances in Applied Mathematics and Mechanics
Adv. Appl. Math. Mech., Vol. **16**, No. 2, pp. 459-492

DOI: 10.4208/aamm.OA-2022-0184
April 2024

New Finite Volume Mapped Unequal-Sized WENO Scheme for Hyperbolic Conservation Laws

Yan Zhang and Jun Zhu*

State Key Laboratory of Mechanics and Control for Aerospace Structures, Nanjing University of Aeronautics and Astronautics, No. 29 Yudao Street, Nanjing, Jiangsu 210016, China

Received 8 July 2022; Accepted (in revised version) 14 February 2023

Abstract. This article designs a new fifth-order finite volume mapped unequal-sized weighted essentially non-oscillatory scheme (MUS-WENO) for solving hyperbolic conservation laws on structured meshes. One advantage is that the new mapped WENO-type spatial reconstruction is a convex combination of a quartic polynomial with two linear polynomials defined on unequal-sized central or biased spatial stencils. Then we propose the new mapped nonlinear weights and new mapping function to decrease the difference between the linear weights and nonlinear weights. This method has the characteristics of small truncation errors and high-order accuracy. And it could give optimal fifth-order convergence with a very tiny ε even near critical points in smooth regions while suppressing spurious oscillations near strong discontinuities. Compared with the classical finite volume WENO schemes and mapped WENO (MWENO) schemes, the linear weights can be any positive numbers on the condition that their summation is one, which greatly reduces the calculation cost. Finally, we propose a new modified positivity-preserving method for solving some low density, low pressure, or low energy problems. Extensive numerical examples including some unsteady-state problems, steady-state problems, and extreme problems are used to testify to the efficiency of this new finite volume MUS-WENO scheme.

AMS subject classifications: 65M60, 35L65

Key words: Mapped WENO scheme, finite volume, unequal-sized stencil, mapping function, steady-state problem, extreme problem.

1 Introduction

In this article, a new fifth-order finite volume mapped unequal-sized weighted essentially non-oscillatory (MUS-WENO) scheme is designed for hyperbolic conservation laws.

---

*Corresponding author.

Emails: yanzhanglut@163.com (Y. Zhang), zhujun@nuaa.edu.cn (J. Zhu)

We first introduce some features of this finite volume MUS-WENO scheme. Different from the classic finite volume high-order WENO scheme [35], a new space reconstruction methodology is used to construct one quartic polynomial and two linear polynomials on unequal-sized spatial stencils. It effectively avoids contact discontinuities or strong shocks that lie in all equal-sized central or biased spatial stencils [35]. And the linear weights can be any positive number that summation to 1, which significantly saves the calculation cost. Based on [23], we design a new mapping function to decrease the difference between the linear weights and nonlinear weights. It could achieve optimal fifth-order accuracy with very tiny ε even near the critical points in smooth regions while having sharp shock transitions in discontinuous regions. This new finite volume MUS-WENO scheme has small numerical errors in L^1 and L^∞ norms inside smooth regions. Finally, this finite volume MUS-WENO scheme with a very tiny ε can compute some unsteady-state problems without losing the designed order of accuracy at critical points in smooth regions, some steady-state problems without introducing big average residue, and some extreme problems containing low density, low pressure, or low energy, respectively.

So far, many numerical schemes were studied for solve compressible hyperbolic conservation laws with various fluid structures. As early as 1984, Colella et al. [6] innovatively designed the piecewise parabolic method that used a four-point central spatial stencil to represent the interfacial values and the values were applied to suppress nonphysical oscillations at discontinuities. In 1991, Leonard [29] proposed the ULTIMATE conservative difference scheme for the first time and effectively solved one-dimensional unsteady advection problems. The results show that the limiting methods could reduce the accuracy from theoretical optimal order to first-order accuracy even at critical points in smooth regions. The idea of the PMM method can be traced back to the MUSCL scheme [39] and Godunov's scheme [15]. The construction of high-order schemes has always been the focus of research. Harten and Osher [22] proposed a new TVD scheme [19] and designed the new ENO schemes. Harten et al. [21] applied the new ENO schemes to simulate 1D hyperbolic conservation laws problems. In the same year, Harten [20] innovatively designed a 2D extension of the ENO schemes. In 1992, Casper [4], and Casper and Atkins [5] presented the ENO schemes for solving hyperbolic conservation laws. In 1994, Liu et al. [33] first designed a third-order finite volume weighted ENO (WENO) scheme based on the ENO scheme. In 1996, Jiang et al. [27] proposed a fifth-order finite difference WENO scheme and extended it to multi-dimensional cases. In 1999, Hu et al. [26] designed the higher-order WENO schemes on unstructured meshes. In 2004, Titarev and Toro [38] designed the finite-volume WENO schemes for solving 3D hyperbolic conservation laws. In 2009, Zhang et al. [46] designed the third-order WENO scheme on the tetrahedral meshes. Due to the construction process of the traditional high-order WENO schemes, the linear weight may have negative values. So, special handling of negative linear weights was required, which increased the computational cost. In 2017, Zhu and Qiu [49] overcame this difficulty.

In 2005, Henrick et al. [23] designed a new mapping function to solve the difficulty that the classic fifth-order WENO scheme [27,35,36] had only third-order accuracy at critical points in smooth regions. The main objective of this mapping function is to modify the nonlinear weights to be the mapped nonlinear weights to obtain the optimal order of accuracy at the critical point in smooth regions. In 2008, Borges et al. [2] proposed an improved WENO scheme to solve the problem of insufficient accuracy of the classic WENO scheme at critical points in smooth regions. In 2012, Feng et al. [11] proposed a new mapped WENO scheme. Their research [23] showed that the mapping function might amplify the effect of non-smooth stencils and produce a loss of accuracy in non-smooth regions. Two years later, Feng et al. [12] designed an improved mapped WENO scheme. In 2006, Bryson et al. [3] designed the mapped weighted power ENO scheme and the WENO scheme to simulate Hamilton-Jacobi equations. In 2013, Gao et al. [13] proposed the finite difference mapped hybrid center-WENO scheme to solve the detonation waves problem. In 2016, Wang et al. [41] proposed the mapped WENO scheme based on the rational mapping function. Two years later, Vevek et al. [40] designed a mapped WENO scheme based on a more general rational mapping function. In 2020, Hong et al. [24] improved the traditional mapping WENO scheme and designed a WENO-M scheme that saved computational cost. It can be seen from the above research results that the introduction of a mapping function can effectively solve the difficulty of the accuracy loss of the classic WENO scheme [27,35,36] at the critical point in smooth regions. When solving extreme problems, the negative density and negative pressure may often emerge in the computing fields. Therefore, it was very important to construct a conservative positivity-preserving method. In 1991, Einfeldt et al. [8] studied the first-order positivity-preserving method. Following the idea of [42], Zhang and Shu [43] designed a general framework for constructing high-order positivity-preserving discontinuous Galerkin methods and finite volume schemes. In 2011, Zhang et al. [44] presented a simpler positivity-preserving method for WENO schemes. And many positivity-preserving methods [9, 10, 16, 25, 45] for solving compressible Euler equations and Navier-Stokes equations have been successfully designed and applied in large-scale engineering applications till now.

In this article, we proposed a new fifth-order finite volume MUS-WENO scheme for solving hyperbolic conservation laws. This finite volume MUS-WENO scheme constructs one quartic polynomial and two linear polynomials on unequal-sized stencils, thereby reducing the difficulty of computing the optimal linear weights. However, the difference between the linear weights and nonlinear weights does not conform to the principle proposed in [27, 35, 36], which leads to the loss of accuracy in smooth regions. Therefore a new mapping function is designed to decrease the difference between the linear weights and the mapped nonlinear weights. It could achieve fifth-order accuracy with a very tiny ε even near critical points in smooth regions. Then we apply a third-order TVD Runge-Kutta method [37] to the time discretization. The MUS-WENO scheme with a new modification of the positivity-preserving method could not only compute some unsteady-state problems or steady-state problems but also compute some extreme problems, such as multi-dimensional Sedov blast wave problems [28, 34] which have strong discontinuities and low density, one-dimensional Leblanc problem [32] which has weak density and strong pressure, and two two-dimensional high Mach number astrophysical jet problems [14, 17, 18] which have low density, low pressure, and low energy, respectively.

The organization of the paper is as follows. In Section 2, a new fifth-order finite volume MUS-WENO scheme is proposed. In Section 3, we design a new modified positivity-preserving method. In Section 4, some classical numerical tests are used to testify to the efficiency of the new finite volume MUS-WENO scheme in simulating some unsteady-state problems, steady-state problems, and extreme problems containing low density, low pressure, or low energy. Finally, the conclusion remarks are presented in Section 5.

2 Finite volume MUS-WENO scheme

We design the MUS-WENO scheme for one-dimensional hyperbolic conservation laws

$$\begin{cases} u_t+f_x(u)=0, \\ u(x,0)=u_0(x). \end{cases} \tag{2.1}$$

The uniform mesh is divided into some cells $I_i=[x_{i-\frac{1}{2}},x_{i+\frac{1}{2}}]$ with uniform cell sizes $x_{i+\frac{1}{2}}-x_{i-\frac{1}{2}}=h$ and the cell centers are $x_i=\frac{1}{2}(x_{i+\frac{1}{2}}+x_{i-\frac{1}{2}})$. We define one-dimensional cell averages as

$$\bar{u}_i(t)=\frac{1}{h}\int_{x_{i-\frac{1}{2}}}^{x_{i+\frac{1}{2}}}u(x,t)dx$$

and use $\bar{w}$ to denote the cell averaging operator in the following. We integrate (2.1) over the target cell $I_i=$ and get the integral formulation

$$\frac{d\bar{u}_i(t)}{dt}=-\frac{1}{h}\Big(f(u(x_{i+\frac{1}{2}},t))-f(u(x_{i-\frac{1}{2}},t))\Big). \tag{2.2}$$

We approximate (2.2) by the following semi-discrete conservative scheme

$$\frac{d\bar{u}_i(t)}{dt}=L(u)_i=-\frac{1}{h}(\hat{f}_{i+\frac{1}{2}}-\hat{f}_{i-\frac{1}{2}}), \tag{2.3}$$

where the numerical flux $\hat{f}_{i+\frac{1}{2}}$ is defined by

$$\hat{f}_{i+\frac{1}{2}}=\hat{f}(u^-_{i+\frac{1}{2}},u^+_{i+\frac{1}{2}}) \tag{2.4}$$

with the values $u^{\pm}_{i+\frac{1}{2}}$ obtained by the finite volume MUS-WENO scheme. We use the Lax-Friedrichs flux

$$\hat{f}(a,b)=\frac{1}{2}[f(a)+f(b)-\alpha(b-a)], \tag{2.5}$$

where $\alpha=max_u|f'(u)|$ is a constant and the maximum is taken over the whole range of u.

For simplicity, the finite volume MUS-WENO reconstruction to get $u^-_{i+\frac{1}{2}}$ to approximate $u(x_{i+\frac{1}{2}},t)$ up to fifth-order is received by applying a reconstruction method with $\bar{w}_j=\bar{u}_j$ for all j that narrated in the following.

Step 1. Select one big stencil $S_1=\{I_{i-2},I_{i-1},I_i,I_{i+1},I_{i+2}\}$. We construct one quartic polynomial $p_1(x)$ based on the cell averages of S_1, which satisfies

$$\frac{1}{h}\int_{I_j}p_1(x)dx=\bar{w}_j,\quad j=i-2,\cdots,i+2. \tag{2.6}$$

Step 2. Select two smaller stencils $S_2=\{I_{i-1},I_i\}$ and $S_3=\{I_i,I_{i+1}\}$. We construct two linear polynomials $p_2(x)$, $p_3(x)$ based on the cell averages of S_2 and S_3, which satisfy

$$\frac{1}{h}\int_{I_j}p_2(x)dx=\bar{w}_j,\quad j=i-1,i, \tag{2.7}$$

and

$$\frac{1}{h}\int_{I_j}p_3(x)dx=\bar{w}_j,\quad j=i,i+1. \tag{2.8}$$

Step 3. Following the approach designed by Levy, Puppo, and Russo for constructing Central WENO schemes [30,31], we rewrite $p_1(x)$ as

$$p_1(x)=d_1\left(\frac{1}{d_1}p_1(x)-\sum_{\ell=2}^{3}\frac{d_\ell}{d_1}p_\ell(x)\right)+\sum_{\ell=2}^{3}d_\ell p_\ell(x). \tag{2.9}$$

The linear weights $d_\ell,\ell=1,2,3$ can be set as any positive numbers on the condition that $\sum_{\ell=1}^{3}d_\ell=1$. This advantage simplifies the complexity of the spatial reconstruction process and significantly reduces the computational cost. Following [7,30,31,47–49], the linear weights in this paper are set as (1) $d_1=0.98$, $d_2=0.01$, and $d_3=0.01$; (2) $d_1=\frac{1}{3}$, $d_2=\frac{1}{3}$, and $d_3=\frac{1}{3}$; (3) $d_1=0.01$, $d_2=0.495$, and $d_3=0.495$.

Step 4. Similar to [1,27,36], we define the smoothness indicators as

$$\beta_\ell=\sum_{n=1}^{l}\int_{I_i}\Delta x^{2n-1}\left(\frac{d^n p_\ell(x)}{dx^n}\right)^2dx,\quad \ell=1,2,3, \tag{2.10}$$

where $l=4$ for $\ell=1$ and $l=1$ for $\ell=2,3$, respectively. The $\beta_\ell,\ell=1,2,3$ are

$$\begin{aligned}\beta_1=&\left(\frac{-8\bar{w}_{i-1}+\bar{w}_{i-2}+8\bar{w}_{i+1}-\bar{w}_{i+2}}{12}\right)^2+\frac{781}{20}\left(\frac{2\bar{w}_{i-1}-\bar{w}_{i-2}-2\bar{w}_{i+1}+\bar{w}_{i+2}}{12}\right)^2\\&+\frac{13}{3}\left(\frac{174\bar{w}_{i-1}-11\bar{w}_{i-2}-326\bar{w}_i+174\bar{w}_{i+1}-11\bar{w}_{i+2}}{260}\right)^2\\&+\frac{1421461}{2275}\left(\frac{-4\bar{w}_{i-1}+\bar{w}_{i-2}+6\bar{w}_i-4\bar{w}_{i+1}+\bar{w}_{i+2}}{24}\right)^2,\end{aligned} \tag{2.11}$$

and

$$\beta_2=(\bar{w}_{i-1}-\bar{w}_i)^2, \tag{2.12a}$$

$$\beta_3=(\bar{w}_i-\bar{w}_{i+1})^2. \tag{2.12b}$$

Step 5. Calculate the mapped nonlinear weights based on the linear weights, the smoothness indicators, and a new mapping function. In this article, we define

$$\Theta=\max\{\beta_1^2,\beta_2^2,\beta_3^2\}. \tag{2.13}$$

Then we define

$$\omega_\ell=\frac{\bar{\omega}_\ell}{\sum_{\ell\ell=1}^3\bar{\omega}_{\ell\ell}},\qquad \bar{\omega}_\ell=d_\ell\left(1+\left(\frac{\Theta^\kappa}{\beta_\ell^\kappa+\varepsilon}\right)^{\frac{1}{\kappa}}\right),\quad \ell=1,2,3, \tag{2.14}$$

where ε is a small positive number to avoid the denominator to become zero. For example, κ is set as eight in this article. If $\beta_\ell=\mathcal{O}(h^2)$, $\ell=1,2,3$ in smooth regions, they satisfy

$$\bar{\omega}_\ell=d_\ell\left(1+\left(\frac{\mathcal{O}(h^{4\kappa})}{\mathcal{O}(h^{2\kappa})+\varepsilon}\right)^{\frac{1}{\kappa}}\right)=d_\ell+\mathcal{O}(h^2),\quad \ell=1,2,3, \tag{2.15}$$

on condition that $\varepsilon\ll\beta_\ell$. Then $\omega_\ell=d_\ell+\mathcal{O}(h^2)$, $\ell=1,2,3$ in smooth regions. Now, we designed a new mapping function. It is monotonically increasing with finite slope and satisfies

$$\begin{aligned}
&g_\ell(0)=0, && g_\ell(1)=1, && g_\ell(d_\ell)=d_\ell,\\
&g_\ell^{(1)}(d_\ell)=0, && g_\ell^{(2)}(d_\ell)=0, && g_\ell^{(3)}(d_\ell)=\frac{6}{(-1+d_\ell)^2}\neq 0.
\end{aligned}$$

So we define

$$g_\ell(\omega)=\frac{\omega d_\ell(d_\ell-1)^2}{d_\ell^3+\omega-2d_\ell^2\omega-\omega^3+\omega d_\ell(3\omega-2)},\quad \ell=1,2,3. \tag{2.16}$$

If $\omega=d_\ell+\mathcal{O}(h^r)$, we get $g_\ell(\omega)=d_\ell+\mathcal{O}(h^{3r})$. Fig. 1 show this new mapping function for three different types of the linear weights. We define

$$\omega_\ell^{(M)}=\frac{g_\ell(\omega_\ell)}{\sum_{k=1}^3 g_k(\omega_k)},\quad \ell=1,2,3. \tag{2.17}$$

If $\varepsilon\ll\beta_k$, we obtain

$$\omega_\ell^{(M)}=d_\ell+\mathcal{O}(h^6),\quad \ell=1,2,3,$$

in smooth regions.

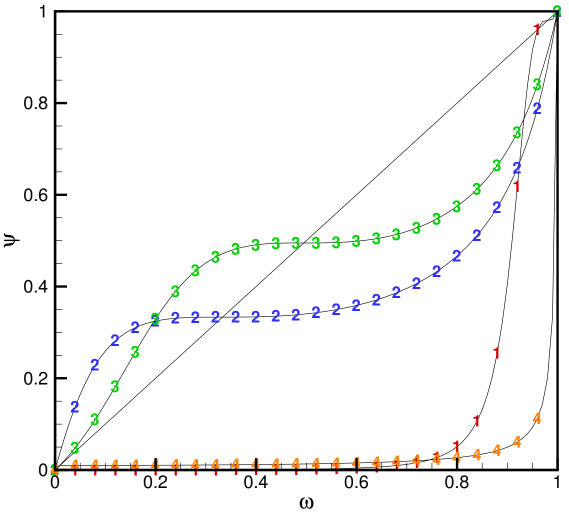

Figure 1: The mapping function with $\Psi = g_\ell(\omega)$, $\ell = 1,2,3$. Solid line: the identity mapping; solid line with the symbol 1: $d = 0.98$; solid line with the symbol 2: $d = 1/3$; solid line with the symbol 3: $d = 0.495$; solid line with the symbol 4: $d = 0.01$.

Step 6. The final reconstruction polynomial $w_i(x)$ is

$$w_i(x) = \omega_1^{(M)} \left(\frac{1}{d_1} p_1(x) - \sum_{\ell=2}^{3} \frac{d_\ell}{d_1} p_\ell(x) \right) + \sum_{\ell=2}^{3} \omega_\ell^{(M)} p_\ell(x). \tag{2.18}$$

Step 7. We use a third-order TVD Runge-Kutta time discretization [37]

$$\left\{ \begin{array}{l} u^{(1)} = u^n + \Delta t L(u^n), \\ u^{(2)} = \frac{3}{4} u^n + \frac{1}{4} u^{(1)} + \frac{1}{4} \Delta t L(u^{(1)}), \\ u^{n+1} = \frac{1}{3} u^n + \frac{2}{3} u^{(2)} + \frac{2}{3} \Delta t L(u^{(2)}), \end{array} \right. \tag{2.19}$$

to solve (2.3) and obtain the final discrete scheme.

Now, we study two-dimensional hyperbolic conservation laws

$$\left\{ \begin{array}{l} u_t + f(u)_x + g(u)_y = 0, \\ u(x,y,0) = u_0(x,y). \end{array} \right. \tag{2.20}$$

The grid mesh is set to uniform cells, and the cell sizes are $h = x_{i+\frac{1}{2}} - x_{i-\frac{1}{2}} = y_{k+\frac{1}{2}} - y_{k-\frac{1}{2}}$, with the cell centers

$$(x_i, y_k) = \left(\frac{1}{2}(x_{i-\frac{1}{2}} + x_{i+\frac{1}{2}}), \frac{1}{2}(y_{k-\frac{1}{2}} + y_{k+\frac{1}{2}}) \right).$$

Define two-dimensional cells

$$I_{i,k}=I_i\times J_k=[x_{i-\frac{1}{2}},x_{i+\frac{1}{2}}]\times[y_{k-\frac{1}{2}},y_{k+\frac{1}{2}}]$$

and cell averages

$$\tilde{\bar{u}}_{i,k}(t)=\frac{1}{h^2}\int_{y_{k-1/2}}^{y_{k+1/2}}\int_{x_{i-1/2}}^{x_{i+1/2}}u(x,y,t)dxdy.$$

We apply $\bar{w}$, $\tilde{w}$ to denote the cell-average operators in the x-direction and y-direction, respectively. We integrate (2.20) over the target cell $I_{i,k}$ and get

$$\begin{aligned}\frac{d\tilde{\bar{u}}_{i,k}(t)}{dt}=&-\frac{1}{h^2}\left(\int_{y_{k-\frac{1}{2}}}^{y_{k+\frac{1}{2}}}f(u(x_{i+\frac{1}{2}},y,t))dy-\int_{y_{k-\frac{1}{2}}}^{y_{k+\frac{1}{2}}}f(u(x_{i-\frac{1}{2}},y,t))dy\right.\\&\left.+\int_{x_{i-\frac{1}{2}}}^{x_{i+\frac{1}{2}}}g(u(x,y_{k+\frac{1}{2}},t))dx-\int_{x_{i-\frac{1}{2}}}^{x_{i+\frac{1}{2}}}g(u(x,y_{k-\frac{1}{2}},t))dx\right).\end{aligned}\tag{2.21}$$

We obtain the semi-discrete conservative form of approximation (2.21)

$$\frac{d\tilde{\bar{u}}_{i,k}(t)}{dt}=L(u)_{i,k}=-\frac{1}{h}(\hat{f}_{i+\frac{1}{2},k}-\hat{f}_{i-\frac{1}{2},k})-\frac{1}{h}(\hat{g}_{i,k+\frac{1}{2}}-\hat{g}_{i,k-\frac{1}{2}}),\tag{2.22}$$

where the numerical fluxes $\hat{f}_{i+\frac{1}{2},k}$ and $\hat{g}_{i,k+\frac{1}{2}}$ are expressed as

$$\hat{f}_{i+\frac{1}{2},k}=\sum_{\ell=1}^{4}\varpi_\ell\hat{f}\big(u^-_{i+\frac{1}{2},k+\sigma_\ell},u^+_{i+\frac{1}{2},k+\sigma_\ell}\big),\tag{2.23a}$$

$$\hat{g}_{i,k+\frac{1}{2}}=\sum_{\ell=1}^{4}\varpi_\ell\hat{g}\big(u^-_{i+\sigma_\ell,k+\frac{1}{2}},u^+_{i+\sigma_\ell,k+\frac{1}{2}}\big),\tag{2.23b}$$

to approximate

$$\frac{1}{h}\int_{y_{k-\frac{1}{2}}}^{y_{k+\frac{1}{2}}}f(u(x_{i+\frac{1}{2}},y,t))dy\quad\text{and}\quad\frac{1}{h}\int_{x_{i-\frac{1}{2}}}^{x_{i+\frac{1}{2}}}g(u(x,y_{k+\frac{1}{2}},t))dx,$$

respectively. ϖ_ℓ and σ_ℓ are 4-point Gauss-Lobatto quadrature weights and nodes in the cell $[-\frac{1}{2},\frac{1}{2}]$. For the numerical fluxes $\hat{f}(a,b)$ and $\hat{g}(a,b)$, we use the simple Lax-Friedrichs flux (2.5). $u^\pm_{i+\frac{1}{2},k+\sigma_\ell}$ and $u^\pm_{i+\sigma_\ell,k+\frac{1}{2}}$ are the fifth-order approximations of $u(x^\pm_{i+\frac{1}{2}},y_{k+\sigma_\ell},t)$ and $u(x_{i+\sigma_\ell},y^\pm_{k+\frac{1}{2}},t)$, respectively.

However, although the building block of the finite volume WENO scheme is still a one-dimensional reconstruction method mentioned above, this method needs to be used multiple times. This way we can "de-cell average" from 2D cell averages $\tilde{\bar{u}}_{i,k}$ to point value $u^\pm_{i+\frac{1}{2},k+\sigma_\ell}$ etc. at different Gauss-Lobatto quadrature points along cell boundaries.

For instance, to get $u^-_{i+\frac{1}{2},k+\sigma_\ell}$ and $u^+_{i-\frac{1}{2},k+\sigma_\ell}$, the procedure is specified in the following. For each k, we assume $\bar{w}_j=\tilde{\bar{u}}_{j,k}$ and apply one-dimensional reconstruction procedure to get $w_i(x)$, then identify

$$\tilde{u}^-_{i+\frac{1}{2},k}=w_i(x_{i+\frac{1}{2}}) \quad \text{and} \quad \tilde{u}^+_{i-\frac{1}{2},k}=w_i(x_{i-\frac{1}{2}}),$$

respectively, which are the y-cell averages of u at $x=x^-_{i+\frac{1}{2}}$ and at $x=x^+_{i-\frac{1}{2}}$, respectively. For each $i+\frac{1}{2}$, we assume $\tilde{w}_j=\tilde{u}^-_{i+\frac{1}{2},j}$ and apply one-dimensional reconstruction procedure to get the polynomial $w_k(y)$, then identify

$$u^-_{i+\frac{1}{2},k+\sigma_\ell}=w_k(y_k+\sigma_\ell h)$$

at all Gauss-Lobatto quadrature points. Similarly, we assume $\tilde{w}_j=\tilde{u}^+_{i-\frac{1}{2},j}$ and apply one-dimensional construction procedure to get the polynomial $w_k(y)$, then identify

$$u^+_{i-\frac{1}{2},k+\sigma_\ell}=w_k(y_k+\sigma_\ell h)$$

at all Gauss-Lobatto quadrature points.

After these point values at associated Gauss-Lobatto quadrature points are received, we could apply (2.22), (2.23) and the third-order TVD Runge-Kutta time discretization (2.19) to get the final discrete scheme. We apply local characteristic decomposition to avoid spurious oscillations in the above reconstruction. This fifth-order finite volume MUS-WENO scheme is easily developed to arbitrarily high-order accuracy, and in a one-dimensional, one-dimensional fashion to multidimensional cases. Since the same linear weights are set at all Gauss-Lobatto integration points on the boundary of the target cell $I_{i,k}$, we could mostly decrease the computation of the spatial reconstruction process compared to the classical finite volume WENO scheme.

3 A new modification of positivity-preserving method

For the good presentation of the classical positivity-preserving method [42–45], it is assumed that the fluid is inviscid and compressible. In this article, for example, one-dimensional Euler equations (2.1) are rewritten as

$$U_t+F(U)_x=0, \tag{3.1}$$

where

$$U=(\rho,m,E)^T \quad \text{and} \quad F(U)=\Big(m,\frac{m^2}{\rho}+p,(E+p)\frac{m}{\rho}\Big)^T.$$

In which ρ is the density, p is the pressure, $m=\rho v$ is the momentum, v is the velocity, E is the total energy, and $\gamma=1.4$ is the ratio of specific heat for the ideal gas. We employ the original idea [43, 44] to design a new modified simple and effective positivity-preserving method to preserve positive density, positive pressure, and positive energy for one-dimensional Euler equations. We first set

$$p(U)=(\gamma-1)\Big(E-\frac{1}{2}\frac{m^2}{\rho}\Big)$$

to be the pressure function. When $\rho>0$, we can easily find that p is a concave function of U. For $U_1=(\rho_1,m_1,E_1)^T$ and $U_2=(\rho_2,m_2,E_2)^T$, Jensen's inequality implies (for $0\le w\le 1$)

$$p(wU_1+(1-w)U_2)\ge wp(U_1)+(1-w)p(U_2), \quad \text{if } \rho_1>0, \quad \rho_2>0. \tag{3.2}$$

We define a set of admissible states as

$$G=\left\{U=\begin{pmatrix}\rho\\ m\\ E\end{pmatrix}:\rho>0 \text{ and } p=(\gamma-1)\left(E-\frac{1}{2}\frac{m^2}{\rho}\right)>0\right\}. \tag{3.3}$$

Then G is a convex set. Our objective is to construct the solutions of the new MUS-WENO scheme in G.

The third-order TVD Runge-Kutta time discretization (2.19) is a convex combination of the Euler forward equations. Since G is convex, we need only discuss the Euler forward time discretization method. The first-order Euler forward time discretization of (3.1) as

$$\bar{U}_i^{n+1}=\bar{U}_i^n-\lambda\big(\hat{F}_{i+\frac{1}{2}}-\hat{F}_{i-\frac{1}{2}}\big), \tag{3.4}$$

where $\lambda=\frac{\Delta t}{h}$. The numerical flux is defined as $\hat{F}_{i+1/2}=\hat{F}(U^-_{i+\frac{1}{2}},U^+_{i+\frac{1}{2}})$ with $U^{\pm}_{i+\frac{1}{2}}$ acquired by the MUS-WENO spatial reconstruction algorithm specified in previous section. $\bar{U}_i^n$ is the approximation to the cell average of the exact solution at time level n. We assume a polynomial vector $Q_i(x)=(\rho_i(x),m_i(x),E_i(x))^T$ on I_i, such that $\bar{U}_i^n$ is the cell average of $Q_i(x)$ on I_i, and

$$U^+_{i-\frac{1}{2}}=Q_i(x_{i-\frac{1}{2}}), \quad U^-_{i+\frac{1}{2}}=Q_i(x_{i+\frac{1}{2}}). \tag{3.5}$$

In this paper, we use 4-point Gauss-Lobatto quadrature on I_i and set the quadrature points such as

$$\{\hat{x}_i^\alpha:\alpha=1,\cdots,4\}=\{x_{i-\frac{1}{2}}=\hat{x}_i^1,\cdots,\hat{x}_i^4=x_{i+\frac{1}{2}}\}.$$

Similar to [43,44], it is well known that $Q_i(\hat{x}_i^\alpha)\in G$ for all i and α is a sufficient condition for $\bar{U}_i^{n+1}\in G$ under suitable CFL conditions. We define $\hat{\omega}_\alpha$ as the Gauss-Lobatto quadrature weights in $[-\frac{1}{2},\frac{1}{2}]$ and $\sum_{\alpha=1}^4\hat{\omega}_\alpha=1$.

Theorem 3.1 ([43,44]). *If* $Q_i(\hat{x}_i^\alpha)\in G$ *for all* i *and* α, *then* (3.4) *is positivity-preserving* ($\bar{U}_i^{n+1}\in G$) *under the CFL condition*

$$\lambda\|(|v|+c)\|_\infty\le\hat{\omega}_1. \tag{3.6}$$

Proof. The cell average $\bar{U}_i^n$ can be written as

$$\bar{U}_i^n=\frac{1}{h}\int_{I_i}Q_i(x)dx=\sum_{\alpha=1}^{4}\hat{\omega}_\alpha Q_i(\hat{x}_i^\alpha).$$

Then we obtain

$$\begin{aligned}\bar{U}_i^{n+1}=&\sum_{\alpha=1}^{4}\hat{\omega}_\alpha Q_i(\hat{x}_i^\alpha)-\lambda\Big(\hat{F}(U^-_{i+\frac{1}{2}},U^+_{i+\frac{1}{2}})-\hat{F}(U^+_{i-\frac{1}{2}},U^-_{i+\frac{1}{2}})+\hat{F}(U^+_{i-\frac{1}{2}},U^-_{i+\frac{1}{2}})-\hat{F}(U^-_{i-\frac{1}{2}},U^+_{i-\frac{1}{2}})\Big)\\ =&\sum_{\alpha=2}^{3}\hat{\omega}_\alpha Q_i(\hat{x}_i^\alpha)+\hat{\omega}_4\left(U^-_{i+\frac{1}{2}}-\frac{\lambda}{\hat{\omega}_4}\left(\hat{F}(U^-_{i+\frac{1}{2}},U^+_{i+\frac{1}{2}})-\hat{F}(U^+_{i-\frac{1}{2}},U^-_{i+\frac{1}{2}})\right)\right)\\ &+\hat{\omega}_1\left(U^+_{i-\frac{1}{2}}-\frac{\lambda}{\hat{\omega}_1}\left(\hat{F}(U^+_{i-\frac{1}{2}},U^-_{i+\frac{1}{2}})-\hat{F}(U^-_{i-\frac{1}{2}},U^+_{i-\frac{1}{2}})\right)\right)\\ =&\sum_{\alpha=2}^{3}\hat{\omega}_\alpha Q_i(\hat{x}_i^\alpha)+\hat{\omega}_4M_4+\hat{\omega}_1M_1,\end{aligned}$$

where

$$\begin{aligned}M_1&=U^+_{i-\frac{1}{2}}-\frac{\lambda}{\hat{\omega}_1}\left(\hat{F}(U^+_{i-\frac{1}{2}},U^-_{i+\frac{1}{2}})-\hat{F}(U^-_{i-\frac{1}{2}},U^+_{i-\frac{1}{2}})\right),\\ M_4&=U^-_{i+\frac{1}{2}}-\frac{\lambda}{\hat{\omega}_4}\left(\hat{F}(U^-_{i+\frac{1}{2}},U^+_{i+\frac{1}{2}})-\hat{F}(U^+_{i-\frac{1}{2}},U^-_{i+\frac{1}{2}})\right).\end{aligned}$$

Since both M_1 and M_4 are two types of (3.4), M_1 and M_4 are in G under the CFL condition (3.6). So we can easily know that $\bar{U}_i^{n+1}$ is in G. □

The vector of approximation polynomials are

$$Q_i(x)=(\rho_i(x),m_i(x),E_i(x))^T,$$

which are reconstructed by the finite volume MUS-WENO scheme. The cell average is $\bar{U}_i^n=(\bar{\rho}_i^n,\bar{m}_i^n,\bar{E}_i^n)\in G$. To achieve positivity-preserving property, we can modify $Q_i(x)$ as

$$\tilde{Q}_i(x)=\theta(Q_i(x)-\bar{U}_i^n)+\bar{U}_i^n, \tag{3.7}$$

on condition that θ is determined by confirming $\rho(\hat{x}_i^\alpha)>0$ and $p(\tilde{Q}_i(\hat{x}_i^\alpha))>0$ at all Gauss-Lobatto points $\hat{x}_i^\alpha$, $\alpha=1,\cdots,4$, respectively. The inequality $p(\tilde{Q}_i(\hat{x}_i^\alpha))>0$ can be rewritten as

$$a_0\theta^2+a_1\theta+a_2>0, \tag{3.8}$$

where

$$\begin{aligned}
&a_0=(\rho_i(\hat{x}_i^\alpha)-\bar{\rho}_i^n)(E_i(\hat{x}_i^\alpha)-\bar{E}_i^n)-\frac{1}{2}(m_i(\hat{x}_i^\alpha)-\bar{m}_i^n)^2,\\
&a_1=\bar{\rho}_i^n(E_i(\hat{x}_i^\alpha)-\bar{E}_i^n)+\bar{E}_i^n(\rho_i(\hat{x}_i^\alpha)-\bar{\rho}_i^n)-\bar{m}_i^n(m_i(\hat{x}_i^\alpha)-\bar{m}_i^n),\\
&a_2=\bar{\rho}_i^n\bar{E}_i^n-\frac{1}{2}(\bar{m}_i^n)^2.
\end{aligned}$$

In the following, we show the flowchart of determining θ in different situations.

(1) Initialize $\theta=1$.

(2) If $\rho_i(\hat{x}_i^\alpha)<0$, then

$$\theta=\min_{\alpha=1,\cdots,4}\left\{\theta,\frac{\bar{\rho}_i^n}{\bar{\rho}_i^n-\rho_i(\hat{x}_i^\alpha)}\right\}. \tag{3.9}$$

(3) If $a_0\neq 0$ and $\Delta=a_1^2-4a_0a_2\geq 0$, we have $\theta_{1,2}=\frac{-a_1\pm\sqrt{\Delta}}{2a_0}$. Then θ is determined according to the distributions of $\theta_{1,2}$. For example, if $a_0>0$, $\Delta\geq 0$, and $\theta_2>\theta_1$,

$$\theta=\begin{cases}\min(\theta,\theta_2), & 0\leq\theta_2<\theta;\\ \min(\theta,\theta_1), & 0\leq\theta_1<\theta<\theta_2;\\ \theta, & \theta_2<0<\theta \quad\text{or}\quad 0<\theta<\theta_1.\end{cases} \tag{3.10}$$

If $a_0<0$, $\Delta\geq 0$, and $\theta_2>\theta_1$,

$$\theta=\begin{cases}\min(\theta,\theta_2), & 0\leq\theta_2<\theta;\\ \min(\theta,\theta_1), & 0\leq\theta_1<\theta<\theta_2;\\ 0, & \theta_2<0<\theta \quad\text{or}\quad 0<\theta<\theta_1.\end{cases} \tag{3.11}$$

If $a_0>0$ and $\Delta<0$, then $\theta=\theta$. If $a_0<0$ and $\Delta<0$, then $\theta=0$.

(4) If $a_0=0$ and $a_1\neq 0$, we have $\theta_3=-\frac{a_2}{a_1}$. Then θ is determined according to the distribution of θ_3. For example, if $a_1>0$,

$$\theta=\begin{cases}\min(\theta,\theta_3), & 0\leq\theta_3<\theta;\\ \theta, & \theta_3<0<\theta;\\ 0, & \theta<\theta_3.\end{cases} \tag{3.12}$$

If $a_1<0$,

$$\theta=\begin{cases}\min(\theta,\theta_3), & 0\leq\theta_3<\theta;\\ 0, & \theta_3<0<\theta;\\ \theta, & \theta<\theta_3.\end{cases} \tag{3.13}$$

(5) If $a_0=0$, $a_1=0$, then θ is determined according to the value of a_2. For example, if $a_2\geq 0$, $\theta=\theta$. If $a_2<0$, $\theta=0$.

Finally, we obtain $\tilde{U}^{\mp}_{i\pm\frac{1}{2}}=\tilde{Q}_i(x_{i\pm\frac{1}{2}})$. Then (3.4) with the positivity-preserving limiter is

$$\bar{U}_i^{n+1}=\bar{U}_i^n-\lambda\left(\hat{F}(\tilde{U}^-_{i+\frac{1}{2}},\tilde{U}^+_{i+\frac{1}{2}})-\hat{F}(\tilde{U}^-_{i-\frac{1}{2}},\tilde{U}^+_{i-\frac{1}{2}})\right). \tag{3.14}$$

Remark 3.1. We describe in detail the design and implementation of a new modified positivity-preserving method for one-dimensional Euler equations. The positivity-preserving method for two-dimensional Euler equations can be deduced in a similar way. Previous positivity-preserving methods required the design of two parameters to achieve the positivity of density and pressure. In this paper, we only need to design only one precise parameter θ, which can keep positive density, positive pressure, and positive energy, respectively. In the next section, we demonstrate the effectiveness of this new modified positivity-preserving method through extensive extreme problems.

4 Numerical results

In this section, the numerical results of the new fifth-order finite volume mapped unequal-sized WENO (MUS-WENO) scheme in comparison to the classical fifth-order finite volume WENO-JS scheme [35], the classical fifth-order finite volume mapped WENO (MWENO) scheme [23], and the fifth-order finite volume WENO-ZQ scheme [48] are presented, respectively. The CFL number is 0.6. We set three different types of the linear weights as: (1) d_1=0.98, d_2=0.01, and d_3=0.01; (2) $d_1=\frac{1}{3}$, $d_2=\frac{1}{3}$, and $d_3=\frac{1}{3}$; (3) d_1=0.01, d_2=0.495, and d_3=0.495, respectively. And we reset the linear weights to be the first type in the other examples unless specified otherwise. When solving some classical steady-state problems, the average residue is defined as

$$Res_A=\sum_{i=1}^{N}\frac{|R1_i|+|R2_i|+|R3_i|+|R4_i|}{4N}, \tag{4.1}$$

where $R*_i$ are local residuals of different conservative variables

$$R1_i=\frac{\partial\rho}{\partial t}\Big|_i\approx\frac{\rho_i^{n+1}-\rho_i^n}{\Delta t},\qquad R2_i=\frac{\partial(\rho u)}{\partial t}\Big|_i\approx\frac{(\rho u)_i^{n+1}-(\rho u)_i^n}{\Delta t},$$
$$R3_i=\frac{\partial(\rho v)}{\partial t}\Big|_i\approx\frac{(\rho v)_i^{n+1}-(\rho v)_i^n}{\Delta t},\qquad R4_i=\frac{\partial E}{\partial t}\Big|_i\approx\frac{E_i^{n+1}-E_i^n}{\Delta t},$$

and N is the total number of grid cells. In this article, we use a single index i to list all grid cells in two dimensions.

Example 4.1. One-dimensional linear advection equation is

$$u_t+u_x=0, \quad -1<x<1, \tag{4.2}$$

with periodic boundary condition and the initial condition

$$u(x,0)=\sin\Big(\pi x-\frac{\sin(\pi x)}{\pi}\Big),$$

and where the exact solution is taken as

$$u(x,t)=\sin\Big(\pi(x-t)-\frac{\sin(\pi(x-t))}{\pi}\Big).$$

The final time is $t=2$. We set $\varepsilon=10^{-40}$ in this example. The numerical errors and orders are computed by the fifth-order finite volume MUS-WENO scheme, WENO-ZQ scheme, MWENO scheme, and WENO-JS scheme in Table 1, respectively. It can be seen that the finite volume MUS-WENO scheme and MWENO scheme could achieve optimal fifth-order accuracy, even in the presence of critical points when ε is a very tiny number. The errors incurred at this level of grid refinement by applying the finite volume WENO-JS scheme and WENO-ZQ scheme with $\varepsilon=10^{-40}$ are not good and the errors are third-order accuracy in the L^∞ norm as shown in Table 1.

Example 4.2. One-dimensional nonlinear Burgers' equation is

$$u_t+\Big(\frac{u^2}{2}\Big)_x=0, \quad x\in(0,2), \tag{4.3}$$

with periodic boundary condition. And the initial condition is $u(x,0)=0.5+\sin(\pi x)$. The final time is $t=0.5/\pi$. The numerical errors and orders are computed by the fifth-order finite volume MUS-WENO scheme, WENO-ZQ scheme, MWENO scheme, and WENO-JS scheme in Table 2, respectively. It can be seen that the finite volume MUS-WENO scheme and MWENO scheme could achieve fifth-order accuracy with $\varepsilon=10^{-40}$ and the former scheme could produce less truncation errors in L^1 and L^∞ norms.

Example 4.3. Two-dimensional nonlinear Burgers' equation is

$$u_t+\Big(\frac{u^2}{2}\Big)_x+\Big(\frac{u^2}{2}\Big)_y=0, \quad x,y\in(0,4), \tag{4.4}$$

with periodic boundary conditions in both directions. And the initial condition is $u(x,y,0)=0.5+\sin(\pi(x+y)/2)$. The final time is $t=0.5/\pi$. The numerical errors and orders of accuracy are computed by the fifth-order finite volume MUS-WENO scheme, WENO-ZQ scheme, MWENO scheme, and WENO-JS scheme in Table 3, respectively. It can be seen that the finite volume MUS-WENO scheme and MWENO scheme could achieve fifth-order accuracy with $\varepsilon=10^{-40}$ and the former scheme could produce less truncation errors in L^1 and L^∞ norms. And the other three different finite volume WENO schemes could not obtain their designed order of accuracy with $\varepsilon=10^{-40}$.

Table 1: $u_t+u_x=0$. MUS-WENO scheme, WENO-JS scheme, WENO-ZQ scheme, and MWENO scheme. $\varepsilon=10^{-40}$. $T=2$.

	MUS-WENO (1) scheme				WENO-JS scheme			
grid cells	L^1 error	order	L^∞ error	order	L^1 error	order	L^∞ error	order
20	2.22E-3		7.29E-3		4.92E-3		1.40E-2	
40	7.24E-5	4.94	1.91E-4	5.25	3.58E-4	3.78	1.09E-3	3.68
60	9.74E-6	4.95	2.66E-5	4.86	6.10E-5	4.36	2.52E-4	3.61
80	2.33E-6	4.97	6.37E-6	4.97	1.70E-5	4.43	9.00E-5	3.58
100	7.67E-7	4.98	2.10E-6	4.97	6.36E-6	4.41	4.11E-5	3.51
120	3.09E-7	4.99	8.48E-7	4.98	2.82E-6	4.45	2.19E-5	3.46
	MUS-WENO (2) scheme				MUS-WENO (3) scheme			
grid cells	L^1 error	order	L^∞ error	order	L^1 error	order	L^∞ error	order
20	3.46E-2		8.31E-2		4.11E-2		9.82E-2	
40	3.54E-4	6.61	1.91E-3	5.44	5.26E-4	6.29	2.71E-3	5.18
60	2.45E-5	6.58	1.31E-4	6.60	3.55E-5	6.65	1.95E-4	6.49
80	5.11E-6	5.46	2.33E-5	6.01	7.29E-6	5.50	3.47E-5	6.00
100	1.56E-6	5.33	6.26E-6	5.89	2.21E-6	5.35	9.34E-6	5.88
120	5.94E-7	5.28	2.26E-6	5.60	8.39E-7	5.31	3.33E-6	5.66
	WENO-ZQ (1) scheme				MWENO scheme			
grid cells	L^1 error	order	L^∞ error	order	L^1 error	order	L^∞ error	order
20	2.30E-3		6.46E-3		1.74E-3		5.13E-3	
40	1.50E-4	3.94	7.88E-4	3.04	6.92E-5	4.65	2.09E-4	4.61
60	2.42E-5	4.51	1.67E-4	3.83	9.56E-6	4.88	2.75E-5	5.00
80	5.02E-6	5.46	2.62E-5	6.43	2.31E-6	4.94	6.57E-6	4.98
100	2.84E-6	2.56	2.39E-5	0.41	7.61E-7	4.97	2.16E-6	4.99
120	1.45E-6	3.68	1.76E-5	1.68	3.07E-7	4.98	8.69E-7	4.99
	WENO-ZQ (2) scheme				WENO-ZQ (3) scheme			
grid cells	L^1 error	order	L^∞ error	order	L^1 error	order	L^∞ error	order
20	2.90E-2		7.07E-2		3.66E-2		8.69E-2	
40	8.68E-4	5.06	4.70E-3	3.91	1.14E-3	5.00	6.19E-3	3.81
60	1.49E-4	4.35	1.14E-3	3.50	1.81E-4	4.55	1.36E-3	3.74
80	3.15E-5	5.41	3.17E-4	4.44	3.91E-5	5.32	3.69E-4	4.53
100	1.49E-5	3.37	1.64E-4	2.95	1.79E-5	3.49	1.88E-4	3.02
120	7.12E-6	4.03	9.38E-5	3.07	8.90E-6	3.84	1.22E-4	2.37

Example 4.4. One-dimensional Euler equations are

$$\frac{\partial}{\partial t}\begin{pmatrix} \rho \\ \rho u \\ E \end{pmatrix}+\frac{\partial}{\partial x}\begin{pmatrix} \rho u \\ \rho u^2+p \\ u(E+p) \end{pmatrix}=0, \tag{4.5}$$

where ρ is the density, p is the pressure, u is the velocity, and E is the total energy with periodic boundary condition. The initial conditions are $\rho(x,0)=1+0.2\sin^6(\pi x)$, $u(x,0)=1$, and $p(x,0)=1$. The exact solution of density is $\rho(x,t)=1+0.2\sin^6(\pi(x-t))$. The computational field is $x\in[0,2]$. The final computing time is $t=2$. The numerical errors and

Table 2: $u_t+(\frac{u^2}{2})_x=0$. MUS-WENO scheme, WENO-JS scheme, WENO-ZQ scheme, and MWENO scheme. $\varepsilon=10^{-40}$. $T=0.5/\pi$.

	MUS-WENO (1) scheme				WENO-JS scheme			
grid cells	L^1 error	order	L^∞ error	order	L^1 error	order	L^∞ error	order
10	7.34E-3		2.15E-2		5.91E-3		1.71E-2	
20	7.69E-4	3.26	4.27E-3	2.34	9.88E-4	2.58	7.13E-3	1.27
40	4.18E-5	4.20	4.33E-4	3.30	8.72E-5	3.50	8.05E-4	3.15
80	1.76E-6	4.57	2.21E-5	4.29	4.13E-6	4.40	4.12E-5	4.29
160	5.97E-8	4.88	7.88E-7	4.81	1.74E-7	4.56	1.52E-6	4.76
320	1.92E-9	4.96	2.53E-8	4.96	7.69E-9	4.50	1.68E-7	3.18
	MUS-WENO (2) scheme				MUS-WENO (3) scheme			
grid cells	L^1 error	order	L^∞ error	order	L^1 error	order	L^∞ error	order
10	3.48E-2		7.97E-2		3.73E-2		8.26E-2	
20	3.82E-3	3.18	2.37E-2	1.75	5.02E-3	2.89	2.74E-2	1.59
40	5.51E-5	6.12	2.87E-4	6.37	6.28E-5	6.32	3.57E-4	6.26
80	1.29E-6	5.41	1.67E-5	4.10	1.21E-6	5.70	1.39E-5	4.68
160	4.39E-8	4.88	6.29E-7	4.73	3.97E-8	4.93	5.49E-7	4.67
320	1.45E-9	4.92	2.04E-8	4.94	1.31E-9	4.92	1.80E-8	4.93
	WENO-ZQ (1) scheme				MWENO scheme			
grid cells	L^1 error	order	L^∞ error	order	L^1 error	order	L^∞ error	order
10	5.39E-3		1.88E-2		2.77E-3		1.04E-2	
20	1.33E-3	2.02	7.51E-3	1.32	6.31E-4	2.13	4.70E-3	1.15
40	5.71E-5	4.54	4.37E-4	4.10	4.26E-5	3.89	4.41E-4	3.41
80	2.84E-6	4.33	2.23E-5	4.29	1.78E-6	4.58	2.23E-5	4.31
160	1.12E-7	4.66	9.04E-7	4.62	6.04E-8	4.88	7.93E-7	4.81
320	5.71E-9	4.30	1.07E-7	3.08	1.94E-9	4.96	2.55E-8	4.96
	WENO-ZQ (2) scheme				WENO-ZQ (3) scheme			
grid cells	L^1 error	order	L^∞ error	order	L^1 error	order	L^∞ error	order
10	3.07E-2		7.26E-2		3.29E-2		7.50E-2	
20	3.22E-3	3.26	1.96E-2	1.89	3.74E-3	3.13	2.32E-2	1.69
40	1.63E-4	4.30	9.65E-4	4.35	1.96E-4	4.25	1.23E-3	4.24
80	7.96E-6	4.36	8.25E-5	3.55	9.61E-6	4.35	1.04E-4	3.56
160	4.05E-7	4.30	9.14E-6	3.17	4.85E-7	4.31	1.17E-5	3.16
320	1.87E-8	4.43	5.28E-7	4.11	2.24E-8	4.44	6.75E-7	4.11

orders of the density are computed by the fifth-order finite volume MUS-WENO scheme, WENO-ZQ scheme, MWENO scheme, and WENO-JS scheme in Table 4, respectively. The finite volume MUS-WENO scheme with $\varepsilon=10^{-40}$ could obtain fifth-order accuracy in smooth regions, and other fifth-order WENO schemes could not achieve their designed order of accuracy with $\varepsilon=10^{-40}$.

Table 3: $u_t+(\frac{u^2}{2})_x+(\frac{u^2}{2})_y=0$. MUS-WENO scheme, WENO-JS scheme, WENO-ZQ scheme, and MWENO scheme. $\varepsilon=10^{-40}$. $T=0.5/\pi$.

	MUS-WENO (1) scheme				WENO-JS scheme			
grid cells	L^1 error	order	L^∞ error	order	L^1 error	order	L^∞ error	order
10× 10	1.05E-2		3.30E-2		6.37E-3		1.77E-2	
20× 20	7.30E-4	3.84	3.20E-3	3.36	8.83E-4	2.85	5.71E-3	1.63
40× 40	3.90E-5	4.23	3.59E-4	3.16	8.21E-5	3.43	6.74E-4	3.08
80× 80	1.70E-6	4.52	2.10E-5	4.09	4.08E-6	4.33	3.91E-5	4.11
160×160	5.93E-8	4.84	7.66E-7	4.78	1.74E-7	4.55	1.42E-6	4.78
320×320	1.91E-9	4.96	2.52E-8	4.93	7.64E-9	4.51	1.54E-7	3.21
	MUS-WENO (2) scheme				MUS-WENO (3) scheme			
grid cells	L^1 error	order	L^∞ error	order	L^1 error	order	L^∞ error	order
10× 10	3.63E-2		9.43E-2		3.91E-2		1.01E-1	
20× 20	4.98E-3	2.87	1.92E-2	2.30	5.97E-3	2.71	2.12E-2	2.25
40× 40	5.71E-5	6.45	3.30E-4	5.86	6.59E-5	6.50	4.81E-4	5.46
80× 80	1.24E-6	5.53	1.60E-5	4.36	1.16E-6	5.83	1.35E-5	5.16
160×160	4.36E-8	4.83	6.04E-7	4.73	3.96E-8	4.87	5.24E-7	4.69
320×320	1.44E-9	4.92	2.03E-8	4.90	1.30E-9	4.93	1.78E-8	4.88
	WENO-ZQ (1) scheme				MWENO scheme			
grid cells	L^1 error	order	L^∞ error	order	L^1 error	order	L^∞ error	order
10× 10	8.76E-3		2.84E-2		3.67E-3		1.59E-2	
20× 20	9.79E-4	3.16	2.99E-3	3.25	4.97E-4	2.89	3.68E-3	2.11
40× 40	5.42E-5	4.18	3.62E-4	3.04	4.00E-5	3.63	3.66E-4	3.33
80× 80	4.52E-6	3.58	4.03E-5	3.17	1.73E-6	4.53	2.21E-5	4.11
160×160	6.94E-8	6.03	7.71E-7	5.71	5.99E-8	4.85	7.71E-7	4.78
320×320	9.27E-9	2.90	3.93E-7	0.97	1.93E-9	4.96	2.53E-8	4.93
	WENO-ZQ (2) scheme				WENO-ZQ (3) scheme			
grid cells	L^1 error	order	L^∞ error	order	L^1 error	order	L^∞ error	order
10× 10	3.21E-2		8.80E-2		3.53E-2		9.24E-2	
20× 20	4.04E-3	2.99	1.59E-2	2.47	4.66E-3	2.92	1.75E-2	2.40
40× 40	2.19E-4	4.20	1.59E-3	3.32	2.57E-4	4.18	1.80E-3	3.28
80× 80	1.04E-5	4.39	1.32E-4	3.59	1.17E-5	4.45	1.52E-4	3.56
160×160	1.96E-7	5.74	5.45E-6	4.60	2.31E-7	5.67	6.65E-6	4.52
320×320	1.83E-8	3.42	9.24E-7	2.56	2.17E-8	3.41	1.19E-6	2.48

Example 4.5. Two-dimensional Euler equations are

$$\frac{\partial}{\partial t}\begin{pmatrix}\rho\\ \rho u\\ \rho v\\ E\end{pmatrix}+\frac{\partial}{\partial x}\begin{pmatrix}\rho u\\ \rho u^2+p\\ \rho uv\\ u(E+p)\end{pmatrix}+\frac{\partial}{\partial y}\begin{pmatrix}\rho v\\ \rho uv\\ \rho v^2+p\\ v(E+p)\end{pmatrix}=0, \tag{4.6}$$

where ρ is the density, p is the pressure, u is the x-directional velocity, v is the y-directional velocity, and E is the total energy with periodic boundary conditions in two directions.

Table 4: One-dimensional Euler equations. MUS-WENO scheme, WENO-JS scheme, WENO-ZQ scheme, and MWENO scheme. $\varepsilon=10^{-40}$. $T=2$.

	MUS-WENO (1) scheme				WENO-JS scheme			
grid cells	L^1 error	order	L^∞ error	order	L^1 error	order	L^∞ error	order
20	2.06E-2		3.46E-2		2.41E-2		5.99E-2	
40	2.84E-3	2.86	6.66E-3	2.38	5.68E-3	2.09	1.58E-2	1.92
60	5.39E-4	4.09	1.24E-3	4.15	1.08E-3	4.09	3.54E-3	3.69
80	1.39E-4	4.71	3.17E-4	4.73	5.18E-4	2.56	1.06E-3	4.19
100	4.70E-5	4.87	1.07E-4	4.87	2.18E-4	3.86	4.16E-4	4.19
120	1.91E-5	4.93	4.35E-5	4.93	9.60E-5	4.51	1.80E-4	4.59
	MUS-WENO (2) scheme				MUS-WENO (3) scheme			
grid cells	L^1 error	order	L^∞ error	order	L^1 error	order	L^∞ error	order
20	2.20E-2		4.29E-2		2.22E-2		4.49E-2	
40	3.13E-3	2.81	7.73E-3	2.47	3.25E-3	2.77	8.18E-3	2.46
60	5.52E-4	4.28	1.35E-3	4.30	5.58E-4	4.34	1.41E-3	4.34
80	1.40E-4	4.76	3.42E-4	4.78	1.41E-4	4.78	3.54E-4	4.80
100	4.73E-5	4.88	1.15E-4	4.89	4.75E-5	4.88	1.19E-4	4.90
120	1.92E-5	4.94	4.65E-5	4.95	1.93E-5	4.94	4.80E-5	4.96
	WENO-ZQ (1) scheme				MWENO scheme			
grid cells	L^1 error	order	L^∞ error	order	L^1 error	order	L^∞ error	order
20	2.05E-2		3.65E-2		2.11E-2		4.40E-2	
40	3.00E-3	2.77	7.23E-3	2.34	1.87E-3	3.49	6.26E-3	2.81
60	5.60E-4	4.14	1.40E-3	4.04	5.08E-4	3.22	1.35E-3	3.79
80	1.43E-4	4.75	4.10E-4	4.28	1.68E-4	3.85	3.75E-4	4.44
100	4.75E-5	4.93	1.47E-4	4.59	6.13E-5	4.51	1.56E-4	3.92
120	1.91E-5	5.00	6.90E-5	4.17	2.50E-5	4.92	6.62E-5	4.72
	WENO-ZQ (2) scheme				WENO-ZQ (3) scheme			
grid cells	L^1 error	order	L^∞ error	order	L^1 error	order	L^∞ error	order
20	2.19E-2		4.60E-2		2.21E-2		4.78E-2	
40	3.69E-3	2.57	1.04E-2	2.14	3.85E-3	2.52	1.11E-2	2.11
60	7.17E-4	4.04	2.57E-3	3.45	7.65E-4	3.98	2.87E-3	3.34
80	1.83E-4	4.75	8.42E-4	3.88	1.97E-4	4.72	9.80E-4	3.73
100	6.17E-5	4.87	3.41E-4	4.05	6.74E-5	4.80	4.06E-4	3.95
120	2.52E-5	4.92	1.67E-4	3.90	2.76E-5	4.89	1.97E-4	3.96

The initial conditions are $\rho(x,y,0)=1+0.2\sin^6(\pi(x+y))$, $u(x,y,0)=1$, $v(x,y,0)=1$, and $p(x,y,0)=1$. The exact solution of density is $\rho(x,y,t)=1+0.2\sin^6(\pi(x+y-2t))$. The computational field is $(x,y)\in[0,2]\times[0,2]$. The final computational time is $t=2$. The numerical errors and orders of density are computed by the fifth-order finite volume MUS-WENO scheme, WENO-ZQ scheme, MWENO scheme, and WENO-JS scheme in Table 5, respectively. The new finite volume MUS-WENO scheme could maintain good numerical results in smooth regions, and the other three WENO schemes could not achieve their designed order of accuracy with $\varepsilon=10^{-40}$ once again.

Table 5: Two-dimensional Euler equations. MUS-WENO scheme, WENO-JS scheme, WENO-ZQ scheme, and MWENO scheme. $\varepsilon=10^{-40}$. $T=2$.

	MUS-WENO (1) scheme				WENO-JS scheme			
grid cells	L^1 error	order	L^∞ error	order	L^1 error	order	L^∞ error	order
20× 20	2.10E-2		4.48E-2		3.42E-2		7.95E-2	
40× 40	4.12E-3	2.35	1.05E-2	2.10	1.31E-2	1.39	3.71E-2	1.10
60× 60	9.23E-4	3.69	2.17E-3	3.88	4.40E-3	2.69	1.19E-2	2.81
80× 80	2.47E-4	4.57	5.71E-4	4.65	2.15E-3	2.48	4.89E-3	3.08
100×100	8.45E-5	4.81	1.94E-4	4.85	1.16E-3	2.76	3.07E-3	2.09
120×120	3.46E-5	4.90	7.90E-5	4.92	6.94E-4	2.83	1.70E-3	3.23
	MUS-WENO (2) scheme				MUS-WENO (3) scheme			
grid cells	L^1 error	order	L^∞ error	order	L^1 error	order	L^∞ error	order
20× 20	2.14E-2		5.22E-2		2.18E-2		5.42E-2	
40× 40	4.42E-3	2.28	1.18E-2	2.14	4.54E-3	2.27	1.24E-2	2.13
60× 60	9.43E-4	3.81	2.35E-3	3.98	9.55E-4	3.85	2.43E-3	4.01
80× 80	2.51E-4	4.60	6.09E-4	4.69	2.53E-4	4.62	6.29E-4	4.70
100×100	8.52E-5	4.84	2.06E-4	4.86	8.56E-5	4.85	2.12E-4	4.86
120×120	3.48E-5	4.91	8.39E-5	4.93	3.49E-5	4.92	8.64E-5	4.94
	WENO-ZQ (1) scheme				MWENO scheme			
grid cells	L^1 error	order	L^∞ error	order	L^1 error	order	L^∞ error	order
20× 20	2.10E-2		4.69E-2		2.75E-2		5.90E-2	
40× 40	4.27E-3	2.29	1.13E-2	2.05	1.07E-2	1.36	3.03E-2	0.96
60× 60	9.61E-4	3.68	2.48E-3	3.75	5.06E-3	1.84	1.58E-2	1.60
80× 80	2.57E-4	4.59	7.16E-4	4.32	2.36E-3	2.65	6.64E-3	3.01
100×100	8.62E-5	4.89	2.39E-4	4.91	1.23E-3	2.94	3.41E-3	2.99
120×120	3.48E-5	4.98	1.09E-4	4.34	7.02E-4	3.06	1.87E-3	3.29
	WENO-ZQ (2) scheme				WENO-ZQ (3) scheme			
grid cells	L^1 error	order	L^∞ error	order	L^1 error	order	L^∞ error	order
20× 20	2.27E-2		5.77E-2		2.34E-2		6.01E-2	
40× 40	4.70E-3	2.27	1.53E-2	1.92	4.84E-3	2.27	1.61E-2	1.90
60× 60	1.21E-3	3.35	4.07E-3	3.26	1.27E-3	3.29	4.53E-3	3.12
80× 80	3.14E-4	4.68	1.32E-3	3.91	3.35E-4	4.64	1.49E-3	3.86
100×100	1.07E-4	4.83	5.27E-4	4.11	1.15E-4	4.80	6.22E-4	3.92
120×120	7.88E-8	4.88	1.43E-6	4.08	4.74E-5	4.85	3.06E-4	3.89

Example 4.6. One-dimensional Euler equations are

$$\frac{\partial}{\partial t}\begin{pmatrix}\rho\\ \rho u\\ E\end{pmatrix}+\frac{\partial}{\partial x}\begin{pmatrix}\rho u\\ \rho u^2+p\\ u(E+p)\end{pmatrix}=0, \tag{4.7}$$

where ρ is the density, p is the pressure, u is the velocity, and E is the total energy with periodic boundary condition. The initial conditions are $\rho(x,0)=1+0.99\sin(x)$, $u(x,0)=1$, and $p(x,0)=1$. The exact solution of density is $\rho(x,t)=1+0.99\sin(x-t)$. The computational field is $x\in[0,2\pi]$. The final computing time is $t=0.1$. The numerical errors and

Table 6: 1D Euler equations: initial data $\rho(x,0)=1+0.99\sin(x)$. MUS-WENO scheme, WENO-JS scheme, WENO-ZQ scheme, and MWENO scheme. $\varepsilon=10^{-40}$. $T=0.1$.

	MUS-WENO (1) scheme				WENO-JS scheme			
grid cells	L^1 error	order	L^∞ error	order	L^1 error	order	L^∞ error	order
20	5.08E-4		8.49E-4		9.81E-4		5.71E-4	
40	1.82E-6	8.13	6.00E-6	7.15	3.03E-5	5.02	1.90E-5	4.91
60	1.32E-7	6.47	5.15E-7	6.05	4.03E-6	4.98	2.53E-6	4.97
80	2.28E-8	6.11	6.57E-8	7.16	9.70E-7	4.95	6.25E-7	4.86
100	7.47E-9	5.00	1.88E-8	5.60	3.17E-7	5.01	2.06E-7	4.97
120	3.00E-9	5.00	7.64E-9	4.95	1.28E-7	5.00	8.26E-8	5.01
	MUS-WENO (2) scheme				MUS-WENO (3) scheme			
grid cells	L^1 error	order	L^∞ error	order	L^1 error	order	L^∞ error	order
20	7.69E-3		1.27E-2		9.67E-3		1.60E-2	
40	4.53E-5	7.41	1.34E-4	6.56	6.66E-5	7.18	1.99E-4	6.33
60	1.50E-6	8.41	5.53E-6	7.86	2.09E-6	8.54	7.81E-6	7.99
80	2.28E-8	14.55	5.43E-8	16.07	2.2E-8	15.71	5.43E-8	17.27
100	7.47E-9	5.00	1.88E-8	4.75	7.47E-9	5.00	1.88E-8	4.75
120	3.00E-9	5.00	7.64E-9	4.95	3.00E-9	5.00	7.64E-9	4.95
	WENO-ZQ (1) scheme				MWENO scheme			
grid cells	L^1 error	order	L^∞ error	order	L^1 error	order	L^∞ error	order
20	2.04E-3		2.07E-3		1.34E-4		6.40E-5	
40	7.56E-5	4.76	1.17E-4	4.15	4.20E-6	5.00	2.10E-6	4.93
60	1.05E-5	4.86	2.12E-5	4.21	5.73E-7	4.91	2.86E-7	4.91
80	8.19E-6	0.88	2.88E-5	-1.06	1.38E-7	4.96	6.88E-8	4.95
100	1.64E-6	7.20	5.39E-6	7.51	4.52E-8	4.99	2.26E-8	4.99
120	6.61E-7	4.99	2.29E-6	4.70	1.82E-8	4.98	9.11E-9	4.99
	WENO-ZQ (2) scheme				WENO-ZQ (3) scheme			
grid cells	L^1 error	order	L^∞ error	order	L^1 error	order	L^∞ error	order
20	9.63E-3		9.82E-3		1.15E-2		1.18E-2	
40	4.16E-4	4.53	6.55E-4	3.91	4.92E-4	4.54	7.80E-4	3.91
60	5.58E-5	4.95	1.15E-4	4.29	6.83E-5	4.87	1.41E-4	4.22
80	3.96E-5	1.19	1.44E-4	-0.78	4.97E-5	1.10	1.81E-4	-0.88
100	1.33E-5	4.88	4.94E-5	4.79	1.68E-5	4.85	6.26E-5	4.77
120	4.06E-6	6.52	1.60E-5	6.18	5.41E-6	6.23	2.14E-5	5.87

orders of the density are computed by the fifth-order finite volume MUS-WENO scheme, WENO-ZQ scheme, MWENO scheme, and WENO-JS scheme in Table 6, respectively. It can be seen that the MUS-WENO scheme, WENO-JS scheme and MWENO scheme could achieve fifth-order accuracy with $\varepsilon=10^{-40}$. But when the grid is dense, the MUS-WENO scheme could produce less truncation errors in L^1 and L^∞ norms.

Example 4.7. Two-dimensional Euler equations are

$$\frac{\partial}{\partial t}\begin{pmatrix}\rho\\ \rho u\\ \rho v\\ E\end{pmatrix}+\frac{\partial}{\partial x}\begin{pmatrix}\rho u\\ \rho u^2+p\\ \rho uv\\ u(E+p)\end{pmatrix}+\frac{\partial}{\partial y}\begin{pmatrix}\rho v\\ \rho uv\\ \rho v^2+p\\ v(E+p)\end{pmatrix}=0, \tag{4.8}$$

where ρ is the density, p is the pressure, u is the x-directional velocity, v is the y-directional velocity, and E is the total energy with periodic boundary conditions in two directions. The initial conditions are $\rho(x,y,0)=1+0.99\sin(x+y)$, $u(x,y,0)=1$, $v(x,y,0)=1$, and $p(x,y,0)=1$. The exact solution of density is $\rho(x,y,t)=1+0.99\sin(x+y-2t)$. The computational field is $(x,y)\in[0,2\pi]\times[0,2\pi]$. The final computational time is $t=0.1$. The numerical errors and orders of density are computed by the fifth-order finite volume MUS-WENO scheme, WENO-ZQ scheme, MWENO scheme, and WENO-JS scheme in Table 7, respectively. It can be seen that the MUS-WENO scheme, WENO-JS scheme and MWENO scheme could achieve fifth-order accuracy with $\varepsilon=10^{-40}$. But when the grid is dense, the MUS-WENO scheme could produce less truncation errors in L^1 and L^∞ norms.

Example 4.8. One-dimensional Sedov blast wave problem [28, 34]. This problem has strong shocks and low density. The initial conditions are $\rho=1$, $u=0$, and $E=10^{-12}$ everywhere except that the energy in the center cell is $\frac{3200000}{\Delta x}$. The computing field is $x\in[-2,2]$. The final time is $t=0.001$. The inlet and outlet conditions are imposed on the left and right boundaries. The classical fifth-order finite volume WENO-JS scheme does not work well for this example. The density, velocity, and pressure computed by the new MUS-WENO scheme are shown in Fig. 2. And the finite volume MUS-WENO scheme with $\varepsilon=10^{-40}$ performs well for this extreme problem.

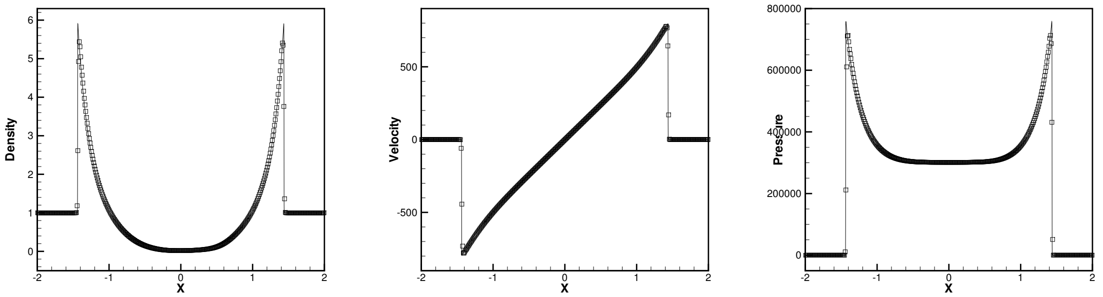

Figure 2: One-dimensional Sedov blast wave problem. $T=0.001$. From left to right: density; velocity; pressure. Solid line: exact solution; squares: MUS-WENO scheme. $\varepsilon=10^{-40}$. 400 grid cells.

Example 4.9. Two-dimensional Sedov problem [28, 34]. The initial conditions are $\rho=1$, $u=0$, $v=0$, and $E=10^{-12}$ everywhere unless the energy is $\frac{0.244816}{\Delta x\Delta y}$ at the lower left

Table 7: 2D Euler equations: initial data $\rho(x,y,0)=1+0.99\sin(x+y)$. MUS-WENO scheme, WENO-JS scheme, WENO-ZQ scheme, and MWENO scheme. $\varepsilon=10^{-40}$. $T=0.1$.

	MUS-WENO (1) scheme				WENO-JS scheme			
grid cells	L^1 error	order	L^∞ error	order	L^1 error	order	L^∞ error	order
20× 20	8.25E-3		2.72E-3		4.08E-3		8.11E-4	
40× 40	2.91E-5	8.15	1.51E-5	7.50	1.44E-4	4.82	3.35E-5	4.60
60× 60	3.33E-6	5.35	1.30E-6	6.05	1.94E-5	4.95	4.81E-6	4.79
80× 80	7.93E-7	4.99	1.53E-7	7.43	4.64E-6	4.97	1.17E-6	4.92
100×100	2.60E-7	4.99	4.14E-8	5.85	1.53E-6	4.98	3.80E-7	5.04
120×120	1.05E-7	4.99	1.67E-8	4.99	6.16E-7	4.99	1.50E-7	5.11
	MUS-WENO (2) scheme				MUS-WENO (3) scheme			
grid cells	L^1 error	order	L^∞ error	order	L^1 error	order	L^∞ error	order
20× 20	6.17E-2		2.01E-2		7.02E-2		2.26E-2	
40× 40	6.20E-4	6.64	3.02E-4	6.05	8.67E-4	6.34	4.30E-4	5.71
60× 60	1.66E-5	8.93	1.21E-5	7.94	2.29E-5	8.96	1.71E-5	7.95
80× 80	7.93E-7	10.57	1.26E-7	15.85	7.93E-7	11.69	1.26E-7	17.07
100×100	2.60E-7	4.99	4.14E-8	4.99	2.60E-7	4.99	4.14E-8	4.99
120×120	1.05E-7	4.99	1.67E-8	4.98	1.05E-7	4.99	1.67E-8	4.98
	WENO-ZQ (1) scheme				MWENO scheme			
grid cells	L^1 error	order	L^∞ error	order	L^1 error	order	L^∞ error	order
20× 20	1.65E-2		5.26E-3		5.90E-4		9.94E-5	
40× 40	3.06E-4	5.75	1.45E-4	5.18	2.03E-5	4.86	4.01E-6	4.63
60× 60	1.39E-4	1.95	9.97E-5	0.93	2.76E-6	4.93	5.56E-7	4.88
80× 80	1.83E-5	7.04	1.74E-5	6.07	6.62E-7	4.96	1.35E-7	4.92
100×100	8.03E-6	3.68	9.06E-6	2.93	2.18E-7	4.97	4.44E-8	4.98
120×120	1.05E-6	11.14	1.53E-6	9.75	8.79E-8	4.99	1.79E-8	4.98
	WENO-ZQ (2) scheme				WENO-ZQ (3) scheme			
grid cells	L^1 error	order	L^∞ error	order	L^1 error	order	L^∞ error	order
20× 20	5.24E-2		1.73E-2		5.67E-2		1.88E-2	
40× 40	2.03E-3	4.69	9.67E-4	4.16	2.42E-3	4.55	1.16E-3	4.02
60× 60	6.00E-4	3.00	4.71E-4	1.77	7.18E-4	2.99	5.62E-4	1.78
80× 80	2.30E-4	3.33	2.38E-4	2.37	2.92E-4	3.12	3.03E-4	2.14
100×100	7.00E-5	5.34	7.66E-5	5.08	8.24E-5	5.67	8.98E-5	5.46
120×120	2.91E-5	4.81	4.18E-5	3.32	3.80E-5	4.25	5.48E-5	2.71

corner. The reflective boundary conditions are applied on the left boundary and the bottom boundary, and the outlet conditions are applied on the right boundary and the top boundary, respectively. The computational time is $t=1$. The results of density computed by the fifth-order finite volume MUS-WENO scheme are shown in Fig. 3. Again, the new finite volume MUS-WENO scheme with $\varepsilon=10^{-40}$ performs well for this extreme problem.

Example 4.10. Two two-dimensional high Mach number astrophysical jet problems [14, 17,18].

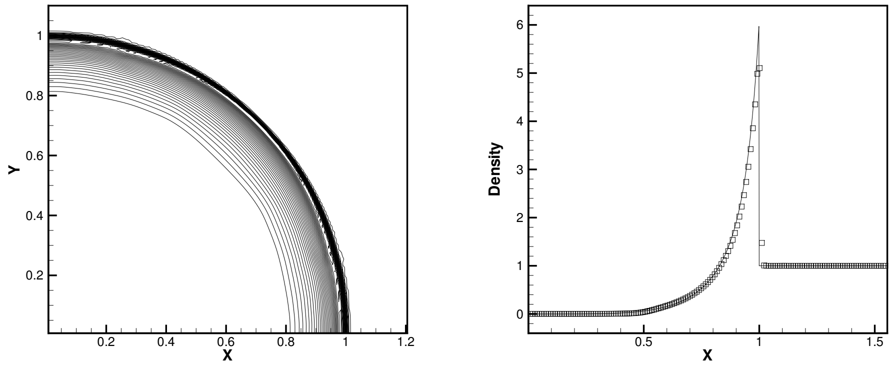

Figure 3: Two-dimensional Sedov problem. $T=1$. From left to right: 30 equally spaced density contours from 0.9 to 5.0; density projects to radial direction. Solid line: exact solution; squares: MUS-WENO scheme. $\varepsilon=10^{-40}$. 160 × 160 grid cells.

(1) A Mach 80 problem. The initial conditions are $(\rho,u,v,p,\gamma)^T=(0.5,0,0,0.4127,5/3)^T$. The computational field is $(x,y)\in[0,2]\times[-0.5,0.5]$. The final time is $t=0.07$. The outflow boundary conditions are used for the right boundary, top boundary, and bottom boundary, respectively. For the left boundary, the initial conditions are

$$(\rho,u,v,p,\gamma)^T=\begin{cases}(5,30,0,0.4127,5/3)^T, & y\in[-0.05,0.05],\\ (0.5,0,0,0.4127,5/3)^T, & \text{otherwise}.\end{cases}$$

The density, pressure, and temperature computed by the new MUS-WENO scheme are shown in Fig. 4.

(2) A Mach 2000 problem. The initial conditions are $(\rho,u,v,p,\gamma)^T=(0.5,0,0,0.4127,\frac{5}{3})^T$. The computational field is $(x,y)\in[0,1]\times[-0.25,0.25]$. The final time is $t=0.001$. The outflow boundary conditions are used for the right boundary, top boundary, and bottom boundary, respectively. For the left boundary, the initial conditions are

$$(\rho,u,v,p,\gamma)^T=\begin{cases}(5,800,0,0.4127,5/3)^T, & y\in[-0.05,0.05],\\ (0.5,0,0,0.4127,5/3)^T, & \text{otherwise}.\end{cases}$$

The density, pressure, and temperature computed by the new MUS-WENO scheme are shown in Fig. 5. It is observed that the finite volume MUS-WENO scheme with $\varepsilon=10^{-40}$ performs well for both extreme problems.

Example 4.11. The shock reflection problem. The computational domain is $(x,y)\in[0,4]\times[0,1]$. The boundary conditions are that of a reflection condition along the bottom boundary and supersonic outflow along the right boundary and Dirichlet conditions on

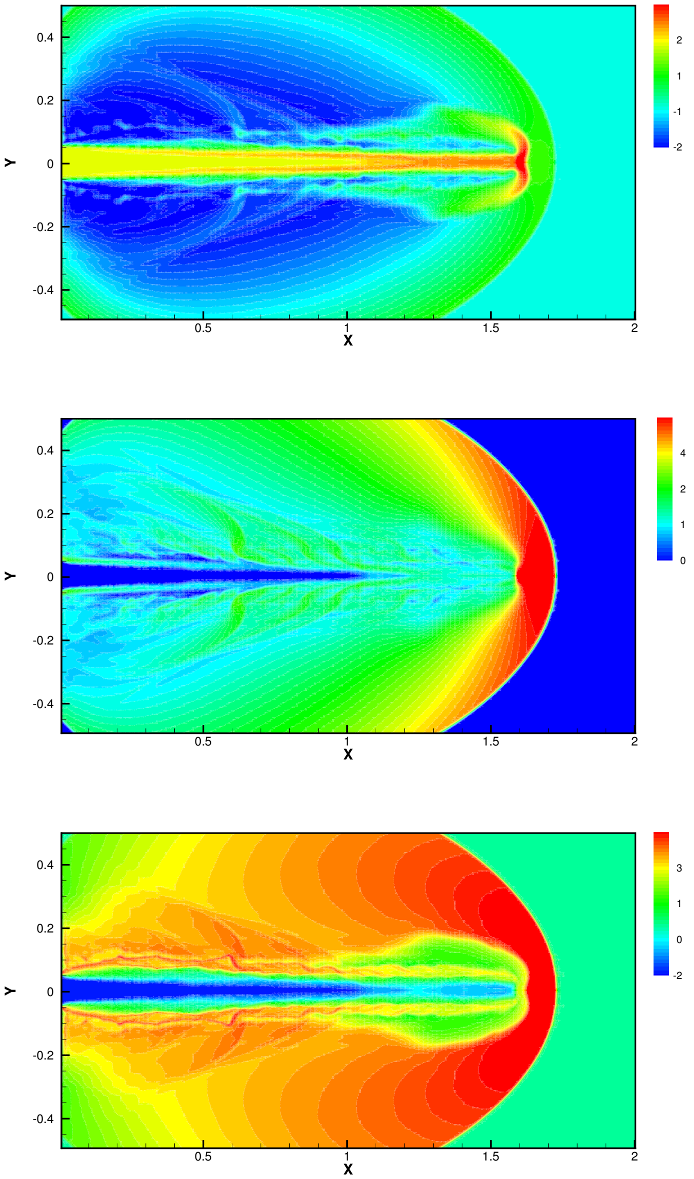

Figure 4: The Mach 80 jet problem. Scales are logarithmic. $T=0.07$. From top to bottom: 40 equally spaced density contours from -2 to 3; 40 equally spaced pressure contours from -0.5 to 5; 40 equally spaced temperature contours from -2 to 4.5. $\varepsilon=10^{-40}$. 448 × 224 grid cells.

the other two sides:

$$(\rho,u,v,p)^T)=\begin{cases} (1.0,2.9,0,1.0/1.4)^T|_{(0,y,t)^T}, \\ (1.69997,2.61934,-0.50632,1.52819)^T|_{(x,1,t)^T}. \end{cases} \tag{4.9}$$

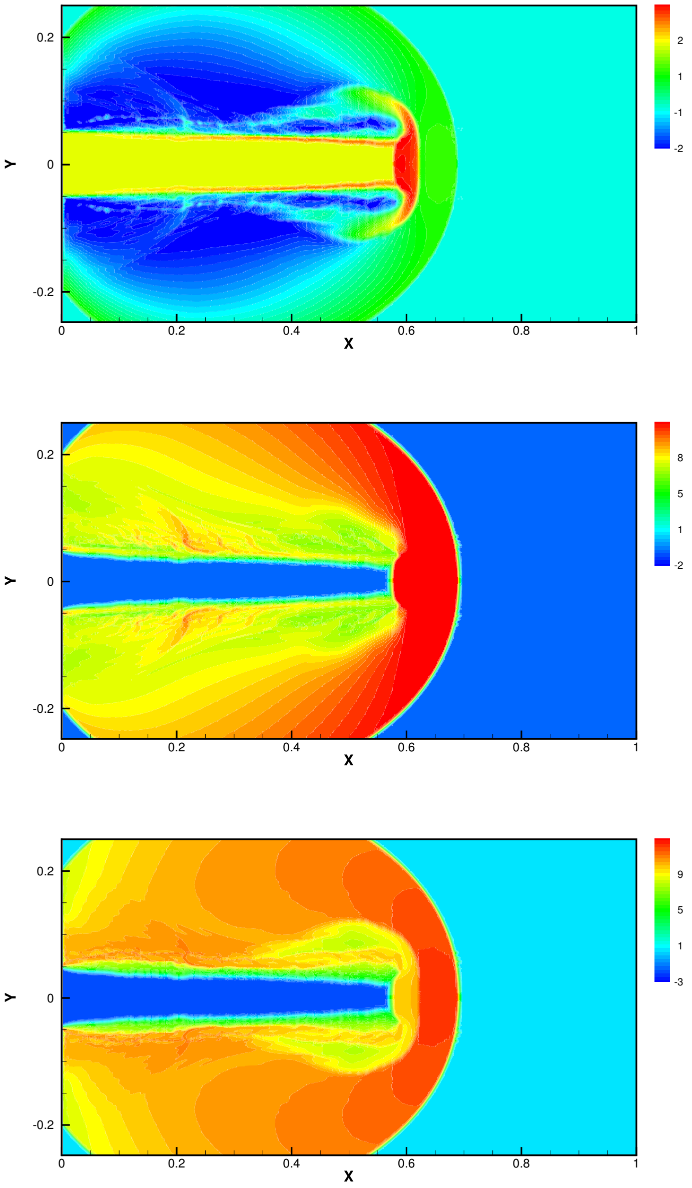

Figure 5: The Mach 2000 jet problem. Scales are logarithmic. $T=0.001$. From top to bottom: 40 equally spaced density contours from -2 to 3; 40 equally spaced pressure contours from -2 to 11; 40 equally spaced temperature contours from -3 to 12.5. $\varepsilon=10^{-40}$. 640 × 320 grid cells.

Initially, the solution for the entire domain is set to the solution for the left boundary. Figs. 6 and 7 show the density contours after numerical steady state is reached. The history of the residue (4.1) as a function of time is also shown in Figs. 6 and 7. The

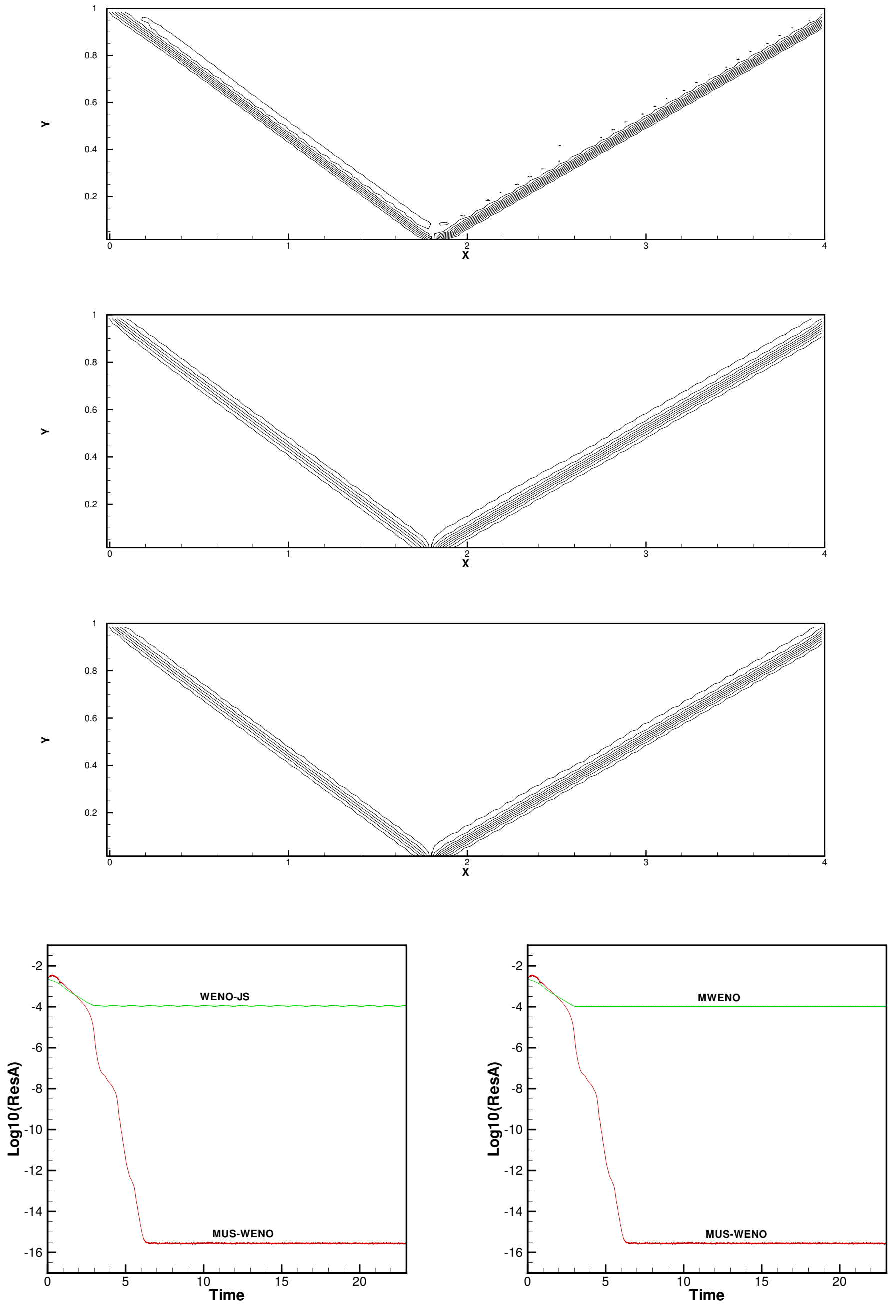

Figure 6: The shock reflection problem. 15 equally spaced density contours from 1.10 to 2.57. From top to bottom: MUS-WENO scheme; WENO-JS scheme; MWENO scheme; the evolution of the average residue. $\varepsilon = 10^{-6}$. 120 × 30 grid cells.

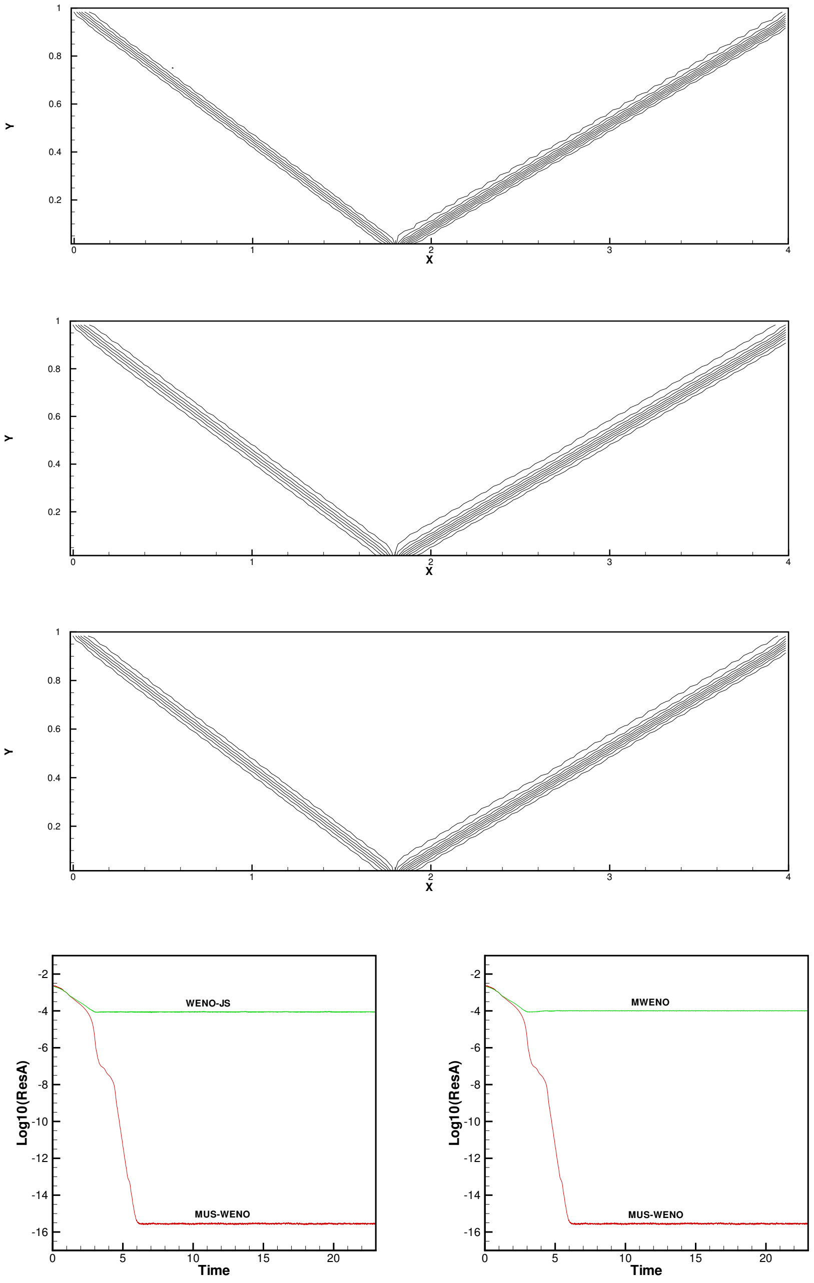

Figure 7: The shock reflection problem. 15 equally spaced density contours from 1.10 to 2.57. From top to bottom: MUS-WENO scheme; WENO-JS scheme; MWENO scheme; the evolution of the average residue. $\varepsilon = 10^{-40}$. 120 × 30 grid cells.

difference between the fifth-order finite volume MUS-WENO scheme, MWENO scheme, and WENO-JS scheme could be easily observed from the residue history. It is obvious that the average residuals of the finite volume WENO-JS scheme and the MWENO scheme with $\varepsilon=10^{-6}$ and $\varepsilon=10^{-40}$ can only drop to a value around 10^{-4}. And the average residuals of the MUS-WENO scheme with $\varepsilon=10^{-6}$ and $\varepsilon=10^{-40}$ can drop to a value around $10^{-15.5}$, close to machine zero.

Example 4.12. A supersonic flow past a two-dimensional plate with an attack angle of $\alpha=15^\circ$ problem. The initial conditions are $p=\frac{1}{\gamma M_\infty^2}$, $\rho=1$, $u=\cos(\alpha)$, and $v=\sin(\alpha)$. We set the free stream Mach number to 3. The ideal gas goes from the left toward the plate. The computational field is $(x,y)\in[0,10]\times[-5,5]$. The plate is set at $x\in[1,2]$ with $y=0$. We impose a slip boundary condition on the plate. Of course the physical values of the inflow and outflow boundary conditions are used in different directions. The numerical results are given when the solutions reach their steady state. Figs. 8 and 9 show the spaced pressure and the time history of the residue (4.1) in the computational domain for the fifth-order finite volume MUS-WENO, WENO-JS, and MWENO schemes. It is obvious that the average residuals of the finite volume WENO-JS scheme [35] and the MWENO scheme [23] with $\varepsilon=10^{-6}$ and $\varepsilon=10^{-40}$ can only drop to a value around 10^{-3}. And the average residuals of the finite volume MUS-WENO scheme with $\varepsilon=10^{-6}$ and $\varepsilon=10^{-40}$

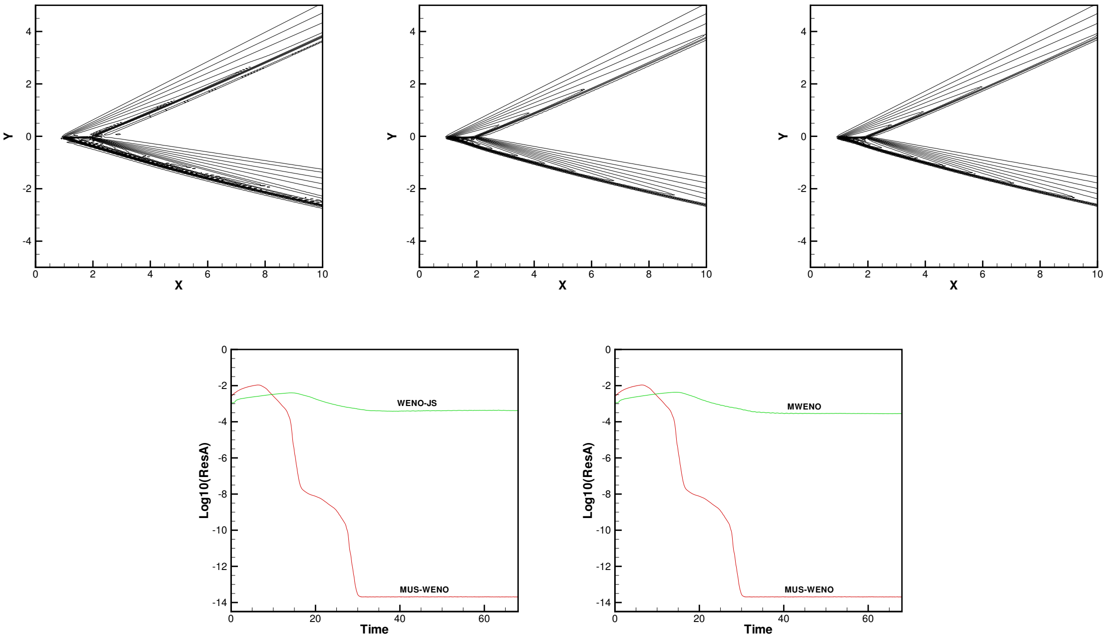

Figure 8: A supersonic flow past a plate problem. 30 equally spaced pressure contours from 0.02 to 0.23. From left to right and top to bottom: MUS-WENO scheme; WENO-JS scheme; MWENO scheme; the evolution of average residue. $\varepsilon=10^{-6}$. 200 × 200 grid cells.

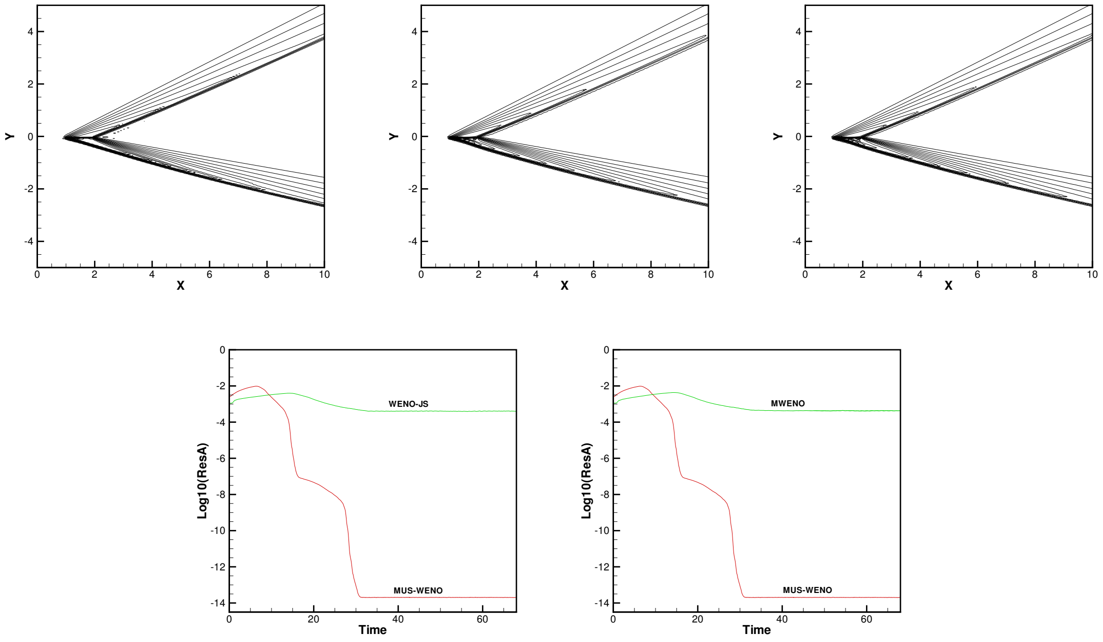

Figure 9: A supersonic flow past a plate problem. 30 equally spaced pressure contours from 0.02 to 0.23. From left to right and top to bottom: MUS-WENO scheme; WENO-JS scheme; MWENO scheme; the evolution of average residue. $\varepsilon=10^{-40}$. 200 × 200 grid cells.

can drop to a value around $10^{-13.5}$, close to machine zero. Although the boundary of this problem is relatively far from the plate, all waves (both shocks and rarefaction waves) propagate towards the far field boundaries. It usually causes the residuals to be difficult to reduce to machine zero for higher-order finite volume schemes, and does not cause any difficulty for the new fifth-order MUS-WENO scheme at all.

Example 4.13. A supersonic flow past two plates with an attack angle of $\alpha=15°$ problem. The initial conditions are $p=\frac{1}{\gamma M_\infty^2}$, $\rho=1$, $u=\cos(\alpha)$, and $v=\sin(\alpha)$. We set the free stream Mach number to 3. The ideal gas goes from the left toward two plates. The computational field is $(x,y)\in[0,10]\times[-5,5]$. Two plates are set at $x\in[2,3]$ with $y=-2$ and at $x\in[2,3]$ with $y=2$. We impose the slip boundary condition on two plates. Of course the physical values of the inflow and outflow boundary conditions are used on the left, right, top, and bottom boundaries, respectively. The numerical results are given when the solutions reach their steady state. Figs. 10 and 11 show the spaced pressure and the time history of the residue (4.1) for the fifth-order finite volume MUS-WENO, WENO-JS, and MWENO schemes. It is obvious that the average residuals of the finite volume WENO-JS scheme [35] and the MWENO scheme [23] with $\varepsilon=10^{-6}$ and $\varepsilon=10^{-40}$ can only drop to a value around 10^{-3}. And the average residuals of the finite volume MUS-WENO scheme with $\varepsilon=10^{-6}$ and $\varepsilon=10^{-40}$ can drop to a value around $10^{-13.5}$, close to machine zero.

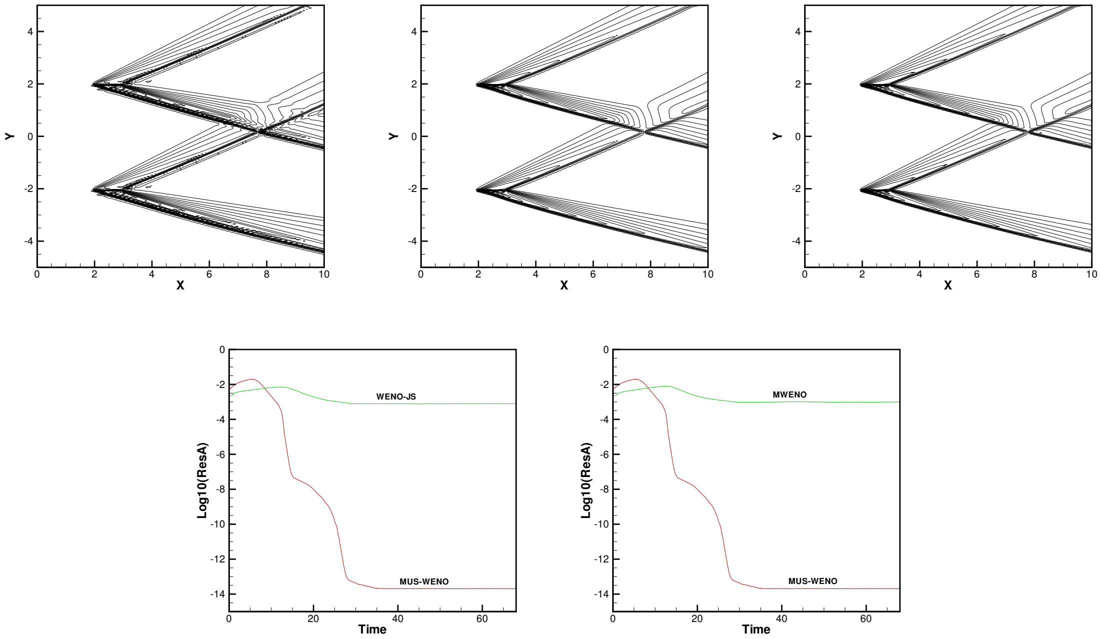

Figure 10: A supersonic flow past two plates problem. 30 equally spaced pressure contours from 0.02 to 0.23. From left to right and top to bottom: MUS-WENO scheme; WENO-JS scheme; MWENO scheme; the evolution of average residue. $\varepsilon = 10^{-6}$. 200 × 200 grid cells.

5 Concluding remarks

In this article, a new fifth-order finite volume MUS-WENO scheme is proposed for solving multi-dimensional hyperbolic conservation laws on structured meshes. The crucial advantages of this finite volume MUS-WENO scheme are its robustness and effectiveness. We use three unequal-sized spatial stencils and can choose any positive linear weights in the process of spatial reconstructions. And we design a new mapping function and reconstruct associated new mapped nonlinear weights. We also design a new positivity-preserving method which is a modification of the classical positivity-preserving methods [42–45]. And this new finite volume MUS-WENO scheme with a very tiny ε can compute some unsteady-state problems without losing the designed order of accuracy at critical points in smooth regions, some steady-state problems without introducing big average residue, and some extreme problems containing low density, low pressure, or low energy, respectively. Extensive benchmark examples are used to verify the good presentations of this new finite volume MUS-WENO scheme. Upcoming work should aim to extend the ideas of this article to compute some steady-state problems and some unsteady-state extreme problems on triangular meshes and tetrahedral meshes.

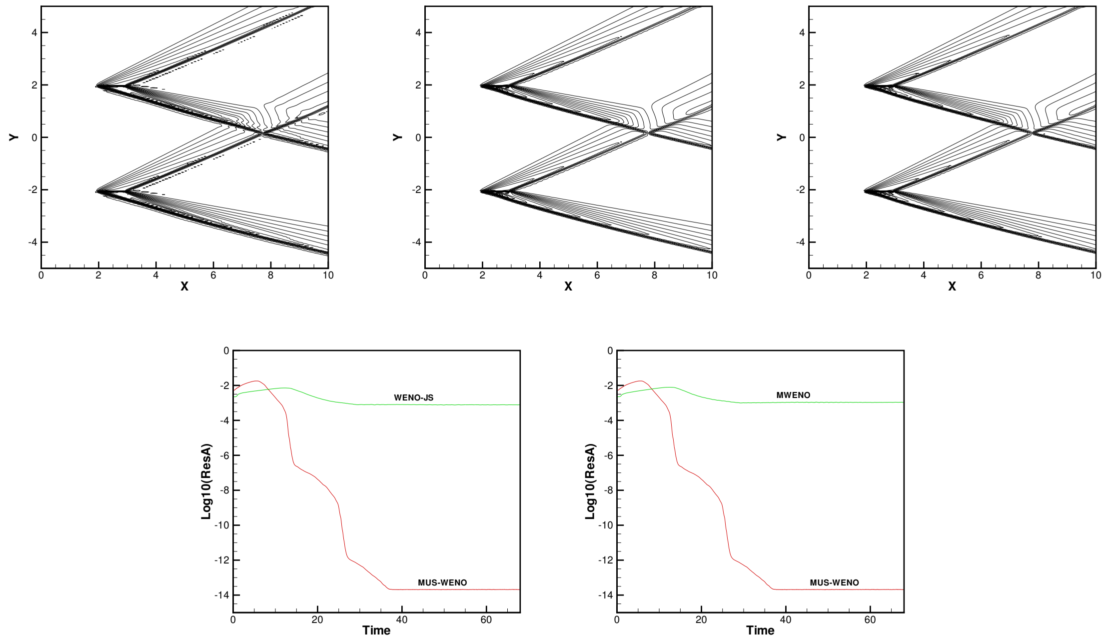

Figure 11: A supersonic flow past two plates problem. 30 equally spaced pressure contours from 0.02 to 0.23. From left to right and top to bottom: MUS-WENO scheme; WENO-JS scheme; MWENO scheme; the evolution of average residue. $\varepsilon=10^{-40}$. 200 × 200 grid cells.

Acknowledgements

The author would like to thank the referees for the helpful suggestions. The first author is supported by National Natural Science Foundation of China (NSFC) grant No. 11872210. The second author is supported by National Natural Science Foundation of China (NSFC) grant No. 11872210 and Grant No. MCMS-I-0120G01.

References

[1] D. S. Balsara, T. Rumpf, M. Dumbser and C. D. Munz, *Efficient, high accuracy ADER-WENO schemes for hydrodynamics and divergence-free magnetohydrodynamics*, J. Comput. Phys., 228 (2009), pp. 2480–2516.

[2] R. Borges, M. Carmona, B. Costa and W. S. Don, *An improved weighted essentially non-oscillatory scheme for hyperbolic conservation laws*, J. Comput. Phys., 227 (2008), pp. 3191–3211.

[3] S. Bryson and D. Levy, *Mapped WENO and weighted power ENO reconstructions in semi-discrete central schemes for Hamilton-Jacobi equations*, Appl. Numer. Math., 56 (2006), pp. 1211–1224.

[4] J. Casper, *Finite-volume implementation of high-order essentially nonoscillatory schemes in two dimensions*, AIAA J., 30 (1992), pp. 2829–2835.

[5] J. CASPER AND H. L. ATKINS, *A finite-volume high-order ENO scheme for two-dimensional hyperbolic systems,* J. Comput. Phys., 106 (1993), pp. 62–76.

[6] P. COLELLA AND P. WOODWARD, *The piecewise parabolic method (PPM) for gas-dynamical simulations,* J. Comput. Phys., 54 (1984), pp. 174–201.

[7] M. DUMBSER AND M. KÄSER, *Arbitrary high order non-oscillatory finite volume schemes on unstructured meshes for linear hyperbolic systems,* J. Comput. Phys., 221 (2007), pp. 693–723.

[8] B. EINFELDT, C. D. MUNZ, P. L. ROE AND B. SJÖGREEN, *On Godunov-type methods near low densities,* J. Comput. Phys., 92 (1991), pp. 273–295.

[9] C. FAN, X. X. ZHANG AND J. X. QIU, *Positivity-preserving high order finite volume hybrid Hermite WENO schemes for compressible Navier-Stokes equations,* J. Comput. Phys., 445 (2021), 110596.

[10] C. FAN, X. X. ZHANG AND J. X. QIU, *Positivity-preserving high order finite difference WENO schemes for compressible Navier-Stokes equations,* J. Comput. Phys., 467 (2022), 111446.

[11] H. FENG, F. X. HU AND R. WANG, *A new mapped weighted essentially non-oscillatory scheme,* J. Sci. Comput., 51 (2012), pp. 449–473.

[12] H. FENG, C. HUANG AND R. WANG, *An improved mapped weighted essentially non-oscillatory scheme,* Appl. Math. Comput., 232 (2014), pp. 453–468.

[13] Z. GAO AND W. S. DON, *Mapped hybrid central-WENO finite difference scheme for detonation waves simulations,* J. Sci. Comput., 55 (2013), pp. 351–371.

[14] C. GARDNER AND S. DWYER, *Numerical simulation of the XZ Tauri supersonic astrophysical jet,* Acta Math. Sci., 29 (2009), pp. 1677–1683.

[15] S. K. GODUNOV, *A finite-difference method for the numerical computation of discontinuous solutions of the equations of fluid dynamics,* Matematicheskii Sbornik, 47 (1959), pp. 271–290.

[16] Y. GUO, T. XIONG AND Y. SHI, *A positivity-preserving high order finite volume compact-WENO scheme for compressible Euler equations,* J. Comput. Phys., 274 (2014), pp. 505–523.

[17] Y. HA AND C. GARDNER, *Positive scheme numerical simulation of high Mach number astrophysical jets,* J. Sci. Comput., 34 (2008), pp. 247–259.

[18] Y. HA, C. GARDNER, A. GELB AND C.-W. SHU, *Numerical simulation of high Mach number astrophysical jets with radiative cooling,* J. Sci. Comput., 24 (2005), pp. 597–612.

[19] A. HARTEN, *High resolution schemes for hyperbolic conservation laws,* J. Comput. Phys., 49 (1983), pp. 357–393.

[20] A. HARTEN, *Preliminary results on the extension of ENO schemes to two-dimensional problems,* in Proceedings, International Conference on Nonlinear Hyperbolic Problems, Saint-Etienne, 1986, Lecture Notes in Mathematics, edited by C. Carasso et al. (Springer-Verlag, Berlin, 1987).

[21] A. HARTEN, B. ENGQUIST, S. OSHER AND S. CHAKRAVARTHY, *Uniformly high order accurate essentially non-oscillatory schemes III,* J. Comput. Phys., 71 (1987), pp. 231–323.

[22] A. HARTEN AND S. OSHER, *Uniformly high-order accurate non-oscillatory schemes,* IMRC Technical Summary Report, 2823, Univ. of Wisconsin, Madison, WI, May 1985.

[23] A. K. HENRICK, T. D. ASLAM AND J. M. POWERS, *Mapped weighted essentially non-oscillatory schemes: achieving optimal order near critical points,* J. Comput. Phys., 207 (2005), pp. 542–567.

[24] Z. HONG, Z. YE AND X. MENG, *A mapping-function-free WENO-M scheme with low computational cost,* J. Comput. Phys., 405 (2020), 109145.

[25] X. Y. HU, N. ADAMS AND C.-W. SHU, *Positivity-preserving method for high-order conservative schemes solving compressible Euler equations,* J. Comput. Phys., 242 (2013), pp. 169–180.

[26] C. HU AND C.-W. SHU, *Weighted essentially non-oscillatory schemes on triangular meshes,* J. Comput. Phys., 150 (1999), pp. 97–127.

[27] G.-S. JIANG AND C.-W. SHU, *Efficient implementation of weighted ENO schemes,* J. Comput. Phys., 126 (1996), pp. 202–228.

[28] V. P. KOROBEINIKOV, Problems of Point-Blast Theory, American Institute of Physics, 1991.

[29] B. P. LEONARD, *The ultimate conservative difference scheme applied to unsteady one-dimensional advection,* Comput. Meth. Appl. Mech. Eng., 88 (1991), pp. 17–74.

[30] D. LEVY, G. PUPPO AND G. RUSSO, *Central WENO schemes for hyperbolic systems of conservation laws,* ESAIM-Math. Model. Numer., 33(3) (1999), pp. 547–571.

[31] D. LEVY, G. PUPPO AND G. RUSSO, *Compact central WENO schemes for multidimensional conservation laws,* SIAM J. Sci. Comput., 22(2) (2000), pp. 656–672.

[32] T. LINDE AND P. L. ROE, *Robust Euler codes,* in: 13th Computational Fluid Dynamics Conference, (1997), AIAA-97-2098.

[33] X. D. LIU, S. OSHER AND T. CHAN, *Weighted essentially non-oscillatory schemes,* J. Comput. Phys., 115 (1994), pp. 200–212.

[34] L. I. SEDOV, Similarity and Dimensional Methods in Mechanics, Academic Press, New York, 1959.

[35] C.-W. SHU, *Essentially non-oscillatory and weighted essentially non-oscillatory schemes for hyperbolic conservation laws,* in: A. Quarteroni, (ed.) Advanced Numerical Approximation of Nonlinear Hyperbolic Equations, Lecture Notes in Mathematics, CIME subseries, Springer, Berlin, (1998).

[36] C.-W. SHU, *High order weighted essentially nonoscillatory schemes for convection dominated problems,* SIAM Rev., 51 (2009), pp. 82–126.

[37] C.-W. SHU AND S. OSHER, *Efficient implementation of essentially non-oscillatory shock capturing schemes,* J. Comput. Phys., 77 (1988), pp. 439–471.

[38] V. A. TITAREV AND E. F. TORO, *Finite-volume WENO schemes for three-dimensional conservation laws,* J. Comput. Phys., 201 (2004), pp. 238–260.

[39] B. VANLEER, *Towards the ultimate conservative difference scheme. V. A second-order sequel to Godunov's method,* J. Comput. Phys., 32 (1979), pp. 101–136.

[40] U. S. VEVEK, B. ZANG AND T. H. NEW, A New Mapped WENO Method for Hyperbolic Problems, in: ICCFD10, Barcelona, Spain, 2018.

[41] R. WANG, H. FENG AND C. HUANG, *A new mapped weighted essentially non-oscillatory method using rational mapping function,* J. Sci. Comput., 67 (2016), pp. 540–580.

[42] X. ZHANG AND C.-W. SHU, *On maximum-principle-satisfying high order schemes for scalar conservation laws,* J. Comput. Phys., 229(9) (2010), pp. 3091–3120.

[43] X. ZHANG AND C.-W. SHU, *On positivity preserving high order discontinuous Galerkin schemes for compressible Euler equations on rectangular meshes,* J. Comput. Phys., 229 (2010), pp. 8918–8934.

[44] X. ZHANG AND C.-W. SHU, *Maximum-principle-satisfying and positivity-preserving high order schemes for conservation laws: Survey and new developments,* Proc. Royal Society A, 467 (2011), pp. 2752–2776.

[45] X. ZHANG AND C.-W. SHU, *Positivity-preserving high order finite difference WENO schemes for compressible Euler equations,* J. Comput. Phys., 231 (2012), pp. 2245–2258.

[46] Y. T. ZHANG AND C.-W. SHU, *Third order WENO scheme on three dimensional tetrahedral meshes,* Commun. Comput. Phys., 5 (2009), pp. 836–848.

[47] X. ZHONG AND C.-W. SHU, *A simple weighted essentially nonoscillatory limiter for Runge-Kutta discontinuous Galerkin methods,* J. Comput. Phys., 232 (2013), pp. 397–415.

[48] J. ZHU AND J. QIU, *A new fifth order finite difference WENO scheme for solving hyperbolic conservation laws,* J. Comput. Phys., 318 (2016), pp. 110–121.

[49] J. ZHU AND J. QIU, *A new type of finite volume WENO schemes for hyperbolic conservation laws,* J. Sci. Comput., 73 (2017), pp. 1338–1359.